JACS
JOURNAL OF THE AMERICAN CHEMICAL SOCIETY

ARTICLE

pubs.acs.org/JACS

Kinetics of Copper Incorporation into a Biosynthetic Purple Cu_A Azurin: Characterization of Red, Blue, and a New Intermediate Species

Tiffany D. Wilson, Masha G. Savelieff, Mark J. Nilges, Nicholas M. Marshall, and Yi Lu*

Department of Chemistry, University of Illinois at Urbana—Champaign, 600 South Mathews Avenue, Urbana, Illinois 61801, United States

Supporting Information

ABSTRACT: Evolutionary links between type 1 blue copper (T1 Cu), type 2 red copper (T2 Cu), and purple Cu_A cupredoxins have been proposed, but the structural features and mechanism responsible for such links as well as for assembly of Cu_A sites in vivo are poorly understood, even though recent evidence demonstrated that the Cu(II) oxidation state plays an important role in this process. In this study, we examined the kinetics of Cu(II) incorporation into the Cu_A site of a biosynthetic Cu_A model, Cu_A azurin (Cu_AAz) and found that both T1 Cu and T2 Cu intermediates form on the path to final Cu_A reconstitution in a pH-dependent manner, with slower kinetics and greater accumulation of the intermediates as the pH is raised from 5.0 to 7.0. While these results are similar to those observed previously in the native Cu_A center of nitrous oxide reductase, the faster kinetics of copper incorporation into Cu_AAz allowed us to use lower copper equivalents to reveal a new pathway of copper incorporation, including a novel intermediate that has not been reported in cupredoxins before, with intense electronic absorption maxima at ~410 and 760 nm. We discovered that this new intermediate underwent reduction to Cu(I), and proposed that it is a Cu(II)−dithiolate species. Oxygen-dependence studies demonstrated that the T1 Cu species only formed in the presence of molecular oxygen, suggesting the T1 Cu intermediate is a one-electron oxidation product of a Cu(I) species. By studying Cu_AAz variants where the Cys and His ligands are mutated, we have identified the T2 Cu intermediate as a capture complex with Cys116 and the T1 Cu intermediate as a complex with Cys112 and His120. These results led to a unified mechanism of copper incorporation and new insights regarding the evolutionary link between all cupredoxin sites as well as the in vivo assembly of Cu_A centers.

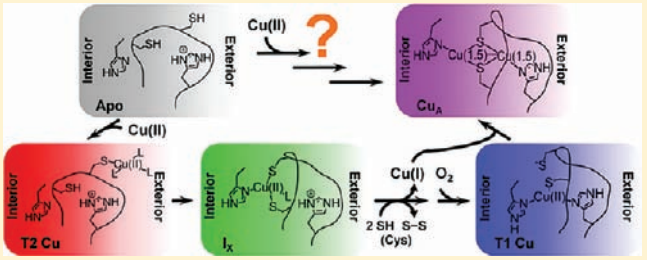

INTRODUCTION

Cupredoxins are a major class of redox and electron transfer (ET) copper proteins that play important roles in diverse biological functions, ranging from photosynthesis to respiration.[1−8] All of them share the same core protein scaffold, called a Greek-key β-barrel (Figure 1a).[6,7] In addition, the copper binding sites of all cupredoxins reside in the same location in the fold and share many common amino acid residues in their primary coordination spheres (Figure 1b). Cysteine thiolate(s), one of the coordinating residue side chains, imparts intense ($\varepsilon \sim 2000-6000\ M^{-1}\ cm^{-1}$) colors to these proteins. One of the types of copper sites is purple Cu_A, which is geometrically distinct from other copper sites, as it forms a rigid diamond core, with two directly bonded coppers bridged by two cysteine (Cys) thiolates.[9−15] Each copper additionally interacts with an equatorial histidine (His) imidazolyl, as well as a weak axial methionine (Met) at one copper and backbone carbonyl oxygen at the other (Figure 1b). In its oxidized resting state, the Cu_A site is mixed valent, with one unpaired electron fully delocalized across the two coppers, giving $[Cu(1.5)\cdots Cu(1.5)]$.[9,16−25] In contrast, mononuclear type 1 (T1) blue copper centers possess a single, strong thiolate ligation from a cysteine, as well as two histidine imidazolyl ligands, completing a nearly trigonal coordination environment around the copper ion, with a fourth ligand (usually methionine) providing weak axial distortion (Figure 1b).[2,26] The type 2 (T2) red copper site exhibits an approximately square pyramidal coordination environment, where the copper ion rests in a plane defined by the Cys thiolate, two imidazolyl nitrogens from His residues, and an exogenous water.[27] Oxygen coordination from the carboxylate of a glutamic acid (Glu) occupies the vertex of the square pyramid (Figure 1b). While the makeup of the primary coordination sphere is similar among the T1 Cu, T2 Cu, and Cu_A sites, their differing geometries give rise to different colors, unique spectral properties, and varied functions.[5,26,28]

Although the dinuclear Cu_A site is different from the mononuclear T1 blue and T2 red Cu centers, phylogenetic analysis has suggested that all three metal ion centers are evolutionarily linked.[31,32] However, direct experimental evidence to support the link is lacking. Recently, we reported the observation of all three types of copper sites (purple Cu_A, T1 blue, and T2 red Cu) in the native, Cu_A-containing nitrous oxide reductase (N_2OR), upon the addition of $CuSO_4$ to the metal-free protein.[33] The T1

Received: June 8, 2011
Published: October 11, 2011

dx.doi.org/10.1021/ja205281t | J. Am. Chem. Soc. 2011, 133, 20778–20792

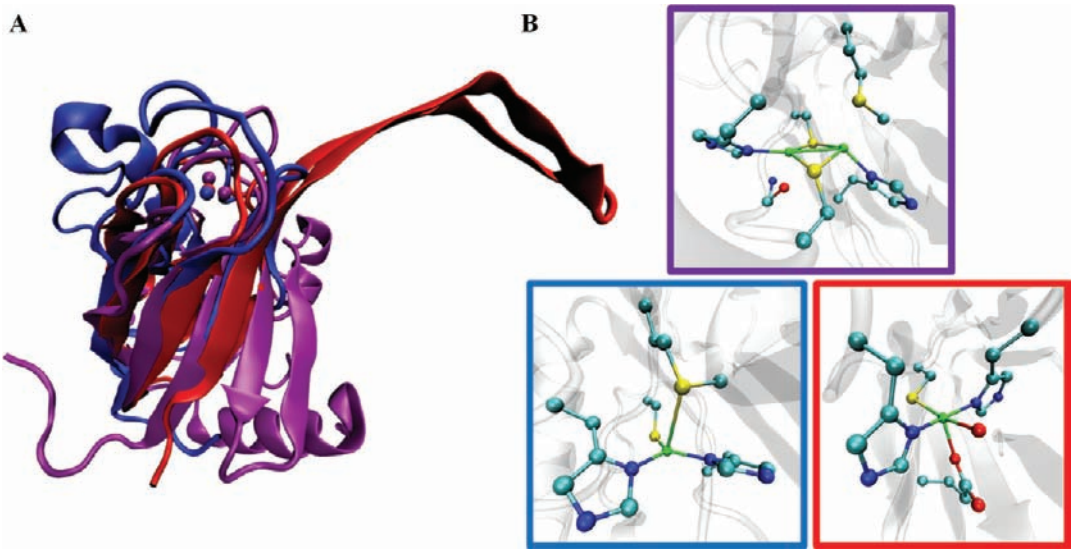

Figure 1. (A) Overlay of the Greek-key β-barrel cupredoxin domains containing Cu_A (purple, *Paracoccus denitrificans* C*c*O, PDB ID code 3HB3), T1 blue Cu (blue, *Pseudomonas aeruginosa* azurin, PDB ID code 1AZU), and T2 red Cu (red, *Nitrosomonas europaea* nitrosocyanin, PDB ID code 1IBY), where copper ions are shown as VDW spheres in the same colors as the corresponding protein backbone. (B) Magnified view of associated active-site structures, with Cu_A shown in a purple box, T1 copper in a blue box, and T2 copper in a red box. The copper sites are shown in ball-and-stick representation, and colors are assigned as follows: cyan for C, blue for N, red for O, yellow for S, and green for Cu. Figures were rendered using VMD software, and structural overlay was performed in the MultiSeq extension of the VMD software.[29,30]

blue and T2 red Cu sites appeared as intermediates on the path to final Cu_A formation, and the process was found to be pH dependent, with more T2 red and T1 blue Cu site accumulation at higher pH. This study constituted the first experimental evidence for the previously proposed evolutionary link between these types of cupredoxins by showing that all three sites are inherently built into the Cu_A site. Despite this report, a question still remains as to whether what was observed in N_2OR is a general feature of other cupredoxins containing Cu_A, as N_2OR contains a tetranuclear Cu_Z center that could contribute to the kinetics of Cu_A formation. More importantly, another intriguing question regarding the Cu_A center is how this valence-delocalized, $[Cu(1.5)\cdots Cu(1.5]$ site can form upon the addition of Cu(II) alone, and what structural features contribute to each of the intermediates. A comprehensive understanding of the kinetics of Cu(II) incorporation into an apo-Cu_A protein, including elucidation of a detailed mechanism, is important not only for establishing a firm evolutionary link between these types of cupredoxins, but also for illuminating features of the in vivo metalation of Cu_A sites.

The mechanism of Cu_A metalation in vivo is not fully understood. In bacteria, the crystal structures of C*c*O show that its Cu_A domain protrudes into the periplasmic or extracellular space,[10,34,35] while the entire N_2OR enzyme is known to be soluble in the periplasm.[36] These environments (periplasmic and extracellular space) are oxidizing relative to the cytoplasm, permitting the Cu(II) oxidation state to exist congruently with Cu(I). Moreover, Sco, a chaperone that plays some role in the biogenesis of Cu_A in C*c*O, was recently demonstrated to require the Cu(II) state for proper function in *Bacillus subtilis*.[37] Therefore, in vivo metalation of Cu_A likely involves Cu(II), and studies of in vitro Cu(II) incorporation into Cu_A sites may provide insight into how and to what extent this oxidation state is useful for this purpose.

The Cu_A center is found in numerous organisms as the electron entry point and transfer hub for aerobic (cytochrome *c* oxidase, C*c*O,[38] and a terminal oxidase, SoxH, in *Sulfolobus acidocaldarius*[39]) and anaerobic (N_2OR[36] and nitric oxide reductase, NOR[40,41]) respiration. Its unique coordination and electron transfer (ET) properties have generated great interest in the Cu_A site.[28,42−49] While the Cu_A center itself is natively found in small cupredoxin-like domains, these domains are associated in some cases with large, membrane-bound complexes[38−40] and always with enzymes containing many other metallochromophores in the as-isolated form, which complicates studies of the Cu_A site.[36,38−40] Thus, several systems have been developed to yield a soluble protein with a Cu_A site that is free from other chromophores, including soluble truncates of native Cu_A proteins[50−56] and biosynthetic models.[57−60] One such biosynthetic model, Cu_A azurin (Cu_AAz), was engineered from the blue copper cupredoxin, azurin, through loop-directed mutagenesis.[59] Extensive spectroscopic, X-ray crystallographic, and electron transfer studies have shown Cu_AAz to be an excellent electronic, structural, and functional model of native Cu_A centers.[13,19,59,61−67]

Herein, we report a study of the incorporation of Cu(II) into Cu_AAz, including explorations of pH dependence and the mechanism of final Cu_A formation. We have found that both T1 blue and T2 red Cu intermediates form on the path to final Cu_A reconstitution in Cu_AAz, as in N_2OR, suggesting the Cu_AAz is also a good model for the kinetics of copper incorporation into Cu_A centers. Moreover, the faster kinetics of copper incorporation into Cu_AAz relative to N_2OR allowed us to use lower copper equivalents, mimicking more closely the limited availability of free copper ions in vivo.[68] Under these copper limiting conditions, a new pathway of copper incorporation was revealed, which included a novel intermediate that has not been reported in cupredoxins before. By studying Cu_AAz variants where the Cys and His ligands were mutated, we have identified ligands responsible for the formation of the intermediates, and elucidated a unified mechanism of copper incorporation. Insights gained from these results on the evolutionary link between all

cupredoxin sites and the relevance to the in vivo metalation of Cu_A sites are discussed.

EXPERIMENTAL SECTION

Materials and Reagents. Bactotryptone and yeast extract were purchased from BD Biosciences. BL-21* (DE3) cells were purchased from Invitrogen. Isopropyl β-D-1-thiogalactopyranoside (IPTG) was purchased from Research Products International Corps or Gold Bio Technology, Inc. All other reagents were purchased from Fisher, Sigma-Aldrich, or Fluka. All water used was purified to 18.2 MΩ cm by ultrafiltration with a Milli-Q Plus PF Ultra-Pure Water System. $CuSO_4$ solutions were prepared volumetrically in water that was incubated with Chelex prior to use. For pH dependent studies, a chelexed universal buffer (UB) containing 40 mM MES, MOPS, Tris, and CAPS, 50 mM NaOAc, and 100 mM $NaNO_3$ (to maintain relatively constant ionic strength) was utilized. For EPR studies, a temperature independent pH (TIP) buffer, previously developed in our laboratory,[69] was used in order to avoid any pH changes upon cooling to 30 K.

Protein Expression, Purification, and Preparation for Experiments. The engineered Cu_A azurin (Cu_AAz) and its C116S and H120A mutants were expressed and purified as previously reported.[59,70,71] Briefly, BL-21* (DE3) cells were transformed with pET-9a plasmid containing the DNA encoding the protein of interest preceded by a periplasmic leader sequence from *P. aeruginosa*. These cells were then grown in 2×YT media at 25 °C and induced with IPTG at $OD_{600} \sim 3$. Cells were allowed to express protein periplasmically at 25 °C for 4 h. After harvesting the cells, lysis of the periplasmic membrane was achieved by osmotic shock. The supernatant after centrifugation was acidified to pH 4.1 with 500 mM sodium acetate, resulting in significant precipitation. After another round of centrifugation, the supernatant was applied to SP Sepharose cation exchange media (GE Healthcare), equilibrated with 50 mM ammonium acetate (NH_4OAc), pH 4.1. A step gradient was applied with 50 mM NH_4OAc, pH 6.35, as the elution buffer, resulting in elution of the desired protein over a broad range to near 100% purity, as determined by polyacrylamide gel electrophoresis. The nearly pure wild-type (wt) or mutant Cu_AAz was then applied to an additional Q-Sepharose HiTrap anion exchange column (GE Healthcare) to remove a minor heme containing contaminant. At this stage, the pH of the protein solution was adjusted to within the buffering range of NH_4OAc (typically pH 5.0−5.5), flash frozen, and stored at −80 °C until required for experiments. When needed for experiments, the appropriate amount of protein was thawed and exchanged into whichever buffer was to be employed for that experiment. Buffer exchanging was typically accomplished by application of the protein to a PD-10 desalting column (GE Healthcare), equilibrated with the buffer of interest. Alternatively, the protein was subjected to several cycles of concentration and dilution with the buffer of interest in a centrifugal filter unit with a 10 kDa molecular weight cutoff (Amicon Ultra from Millipore). The protein was then concentrated to the desired level for the experiment, and the concentration confirmed based on A_{280} using $\varepsilon_{280} = 8440\ cm^{-1}\ M^{-1}$.

Titrations of Cu_AAz with $CuSO_4$. For these experiments, electronic absorption spectra were collected on an Agilent Cary 5000 UV-Vis-NIR spectrophotometer with a mounted Peltier temperature-control unit. Titrations of apoCu_AAz with $CuSO_4$ to saturation (i.e., no further changes in the absorbance at 485 nm with further copper additions) were conducted in UB at 10 °C (Supporting Information Figure S1). To 90 μL of ∼0.25 mM protein in a 1 cm path length quartz cuvette, 3 μL additions of 1 mM $CuSO_4$ were made with mixing immediately after the addition by pipetting the mixture a few times. These additions were repeated until the absorptions due to Cu_A saturated. Once this point had been reached, the protein/copper mixture was covered to prevent evaporation and incubated at 10 °C overnight, while monitoring the electronic absorption spectrum every 20 min. Actual protein concentrations were verified by the absorbance at 280 nm.

In a titration experiment designed to eliminate spectral differences due to kinetic processes (Figure S2), increasing amounts of $CuSO_4$ were added to separate aliquots of protein, and the UV−vis spectrum was collected at 5 min and 18 h after $CuSO_4$ addition. To 10 separate microtubes, 90 μL of ∼0.2 mM apoCu_AAz in UB was added. Incremented equivalents of $CuSO_4$ were added to these microtubes, from ∼0.10 up to 1.0 equiv, using a 2 mM $CuSO_4$ stock, so that 1 μL corresponded to ∼0.1 equiv. The difference between the cumulative volume of apoCu_AAz and $CuSO_4$ and 100 μL was made up with buffer, in order to avoid dilution effects. Immediately after making the $CuSO_4$ addition, the mixture was vortexed and a spectrum collected (i.e., the 5 min spectrum). These samples were then incubated overnight in a 10 °C water bath and a spectrum was collected the following day (i.e., the 18 h spectrum). Actual protein concentrations were verified by the absorbance at 280 nm.

Stopped-Flow UV−Vis Absorbance. Experiments were performed on an Applied Photophysics Ltd. (Leatherhead, U.K.) SX18.MV stopped-flow spectrometer equipped with a 256 element photodiode array detector. Two-syringe mixing was employed to mix equal volumes of H120A or wt Cu_AAz with volumetrically prepared $CuSO_4$ solutions. All reported data sets originally consisted of 200 spectra collected over 50 or 1000 s using logarithmic sampling. The integration period and minimum sampling period were both 1 ms. A water bath, connected to the syringe compartment and set to 15 °C, provided temperature control. The actual temperature in the syringe compartment was measured to be between 16.3 and 16.5 °C. The instrument was prepared for anaerobic stopped-flow by rinsing its lines out several times with buffer that had been degassed by bubbling argon gas through it. Special glass outer syringes fit with Teflon stoppers into which an argon line was run maintained an oxygen free environment. The protein was degassed on a Schlenk line using standard techniques. The copper solutions were degassed either on the Schlenk line or by bubbling with argon gas for 20 min in containers with only a small opening, to allow gases to escape. Oxygen-rich stopped-flow was accomplished by bubbling pure oxygen gas through the $CuSO_4$ solution for 20 min.

Subsaturating $CuSO_4$ Additions to Cu_AAz. Subsaturating $CuSO_4$ additions were made to Cu_AAz and the resulting UV−vis absorbance spectra monitored on an Agilent 8453 photodiode array spectrometer having a connected water bath for temperature control and water-propelled magnetic stirring. After blanking the instrument with a 1:1 mixture of UB/water in a 1 cm × 1 cm standard UV−vis cuvette, 850 μL of 0.5 mM apoCu_AAz was added to the cuvette. The instrument was then set to collect a series of spectra over 3600 s (pH 5) or 900 s (pH 6 and 7) with 0.5 s scan time incremented by 5% after 45 s. After starting the data collection, and with constant magnetic stirring and temperature control set to 10 °C, an 850 μL aliquot of 0.2 mM $CuSO_4$ was quickly added to the stirring protein solution. The top of the cuvette was sealed with Parafilm once data collection was underway to reduce evaporation. For the pH 6 and 7 experiments, spectra were collected for an additional 14 h, with 600 s scan time incremented by 1% after 3600 s.

Electron Paramagnetic Resonance (EPR) Spectroscopy. EPR data collection was performed using an X-band Varian E-122 spectrometer at the Illinois EPR Research Center (IERC). The temperature was set to 30 K using liquid He and an Air Products Helitran cryostat. Frequencies were measured with an EIP frequency counter, and magnetic fields were calibrated with a Varian NMR gaussmeter.

Freeze quench samples were prepared by mixing a 6 mM apoCu_AAz solution in TIP buffer, pH 7 in a 2:1 volume ratio with an 1.2 mM $CuSO_4$ solution, containing 40% glycerol by volume, at room temperature, using an Update Instruments System 1000 equipped with a Wiskind Grid Mixer, a spraying nozzle, and a stirred isopentane bath, cooled by liquid nitrogen to approximately −130 °C. The mixture was passed through a

delay hose of appropriate length to give the desired quench time (for the 100 ms sample), or to yield enough overall sample with four injection/delay cycles (for the 1, 5, and 10 s samples). The sample was frozen by spraying into approximately −130 °C spectrophotometric grade isopentane in a Pyrex collection funnel attached to the EPR tube. Using pre-cooled packing rods and long needles for breaking up improperly packed sample, the frozen sample was packed into the base of the EPR tube, while being maintained at −130 °C. After packing, the samples were transferred to a Dewar containing liquid nitrogen and stored this way until collection of the EPR spectra.

The longer time frame (30 s, 7 min, 15 min, 30 min, and 24 h) Cu_AAz and C116S Cu_AAz in TIP buffer, pH 7 samples were prepared with 30% glycerol as a glassing agent. To achieve reasonably fast mixing for the Cu_AAz sample, 350 μL of the 4 mM apoCu_AAz/glycerol solution was added rapidly by syringe to ∼20 μL of a 7.2 mM $CuSO_4$ solution in the bottom of an EPR tube, syringe mixed, and flash frozen in liquid N_2 in as short a time as possible.

EPR spectra were simulated with SIMPOW6.[72] As the 100 ms sample appeared to be homogeneous, it was simulated as a single species. The time dependent spectra were simulated assuming the presence of four components which were simultaneously fit to minimize the total rms difference between the experimental and simulated spectra.

Global Analysis of Stopped-Flow UV−Vis Absorbance Kinetics Data. As the kinetics in Figure 2 and Figure 4 are generally complex, with multistep reactions and overlapping absorption bands, kinetic analyses were performed using a global analysis software called SpecFit/32 (Spectrum Software Associates, Inc.), which employs singular value decomposition (SVD) and nonlinear regression modeling to find kinetic parameters for the data. Briefly, models were determined through an iterative approach, where the starting point was the simplest conceivable set of reactions that could possibly explain the sequence of events observed in the spectra, while being consistent with other sources of data, and complexity was added as needed to improve the fit and consistency of the models. Fixed or known spectra were required in some cases for the fits to converge (Tables S1 and S2, Figures S3−S6). The quality of these fits was judged based on the size of the standard deviations for the observed rate constants, the reasonableness of the resolved species spectra found by the software (Figures S7−S12), and the statistical measures calculated by the software for each fit. Statistical measures indicating the quality of all of the fits in Scheme 1 are provided as Supporting Information (Figures S13−S18, Tables S1 and S2).

RESULTS

Addition of $CuSO_4$ to apoCu_AAz under Copper Saturating or Subsaturating Conditions. To probe the formation of intermediates during copper incorporation into the Cu_A site, Cu_AAz at pH 5, 6, and 7 was titrated in small increments with $CuSO_4$ in the same aliquot of the protein until no further absorbance increases were observed in the Cu_A absorption bands at 480, 530, and 760−800 nm, and the resulting spectra under these copper-saturating conditions were monitored over time (Figure S1). At pH 5, only the absorptions due to Cu_A were observed. As the pH was raised from pH 5, new absorption bands at ∼400 and 600 nm, assignable tentatively to T2 red Cu and T1 blue Cu species, respectively, were observed, with greater accumulation of these intermediates at lower equivalents of $CuSO_4$ and higher pH. These results are similar to those of native N_2OR,[33] except that isosbestic points between the T1 blue Cu species and Cu_A are not obvious. Therefore, other conditions were investigated, where the T1 blue Cu species might participate in final Cu_A site formation, including lower equivalents of $CuSO_4$. To eliminate spectral differences due to kinetic processes, titrations of Cu_AAz with $CuSO_4$ were repeated, where increasing equivalents of copper were added to separate aliquots of the protein and spectra were collected at the same interval after copper addition (Figure S2). With Cu_A formation monitored at the most intense S → Cu charge transfer band (∼480 nm), the process was complete by ∼0.5 mol equiv of $CuSO_4$ at all pH values. This result was consistent with the hypothesis that, in the absence of external reductants, at least half of the proteins, assuming 100% efficiency, must serve as sacrificial reductants through formation of disulfide bonds between the two active site Cys residues, leaving at most half of the protein available for Cu_A formation. We further confirmed this hypothesis by repeating the same experiment as in Figure S2 using an equimolar mixture of Cu(I) and Cu(II) (Figure S19). Titration with the Cu(I)/Cu(II) mixture resulted in greater Cu_A reconstitution at higher copper equivalents, based upon the absorbance at 480 nm, supporting that the active site thiols supply reducing equivalents when Cu(II) is added. Therefore, to avoid excess copper ions that could complicate the kinetics, we chose to add subsaturating 0.4 equiv amounts of $CuSO_4$ to apo-Cu_AAz in the subsequent experiments.

pH-Dependent Copper Incorporation into Apo-Cu_AAz. Addition and rapid mixing of subsaturating 0.4 equiv of $CuSO_4$ with 0.25 mM apo-Cu_AAz at pH 5 in the stopped-flow apparatus resulted in the UV−vis absorbance spectra in Figure 2A over the following 1000 s. The concentration profiles obtained for these kinetic data based on global analysis are shown in Figure 2B. Spectra corresponding to each of the intermediates and Cu_A, as well as the kinetic models yielding optimal fits with associated observed rate constants, are summarized in Scheme 1. First, a spectrum with an intense absorbance maximum at ∼385 nm, typical of a T2 Cu center with Cys coordination, appeared within 0.3 s. A spectrum very similar to this one was observed previously as an intermediate during formation of Cu_A at pH 5 with higher equivalents of copper.[73] This initial $CuSO_4$ to T2 Cu step was too rapid to be captured in the same data set as some of the slower processes (i.e., in the 1000 s set of spectra), so this process was fit separately, using the beginning portion of a data set collected over 50 s (Figure S20). The rates for this initial $CuSO_4$ to T2 Cu step from global analysis are also included in Scheme 1. In the present study, this ∼385 nm peak subsequently decayed and shifted to ∼410 nm, with absorption bands at 475, 625, and 760 nm growing in intensity over the same time period. This process completed in ∼3 s after addition of copper, and the spectrum observed at its conclusion is associated with a new intermediate, called intermediate X (I_X) here, which is characterized by intense absorption maxima at ∼410 and 760 nm (Scheme 1). Over the next 6.5 s, the absorptions due to I_X decreased, while the shoulder at ∼625 nm intensified slightly and shifted to ∼620 nm, suggesting moderate accumulation of a T1 blue Cu intermediate. Beyond 9.4 s, the absorption bands associated with I_X continued to decay, and the intensity of the shoulder at ∼620 nm also diminished, while a spectrum with absorption maxima at ∼480, 530, and 760 nm emerged; such a spectrum is typical of the Cu_A center in Cu_AAz.[59,61] An isosbestic point at 580 nm was present between the spectrum of T1 blue Cu and that of Cu_A during this final time frame, implying conversion of the T1 blue Cu intermediate to Cu_A.

To find a condition that could maximize formation, and thus characterization, of the intermediate(s) observed during incorporation of copper into apo-Cu_AAz, the experiment shown in Figure 2A,B was repeated at higher pH conditions (see Figure 2C−F). At pH 6, the initial events observable by UV−vis absorbance

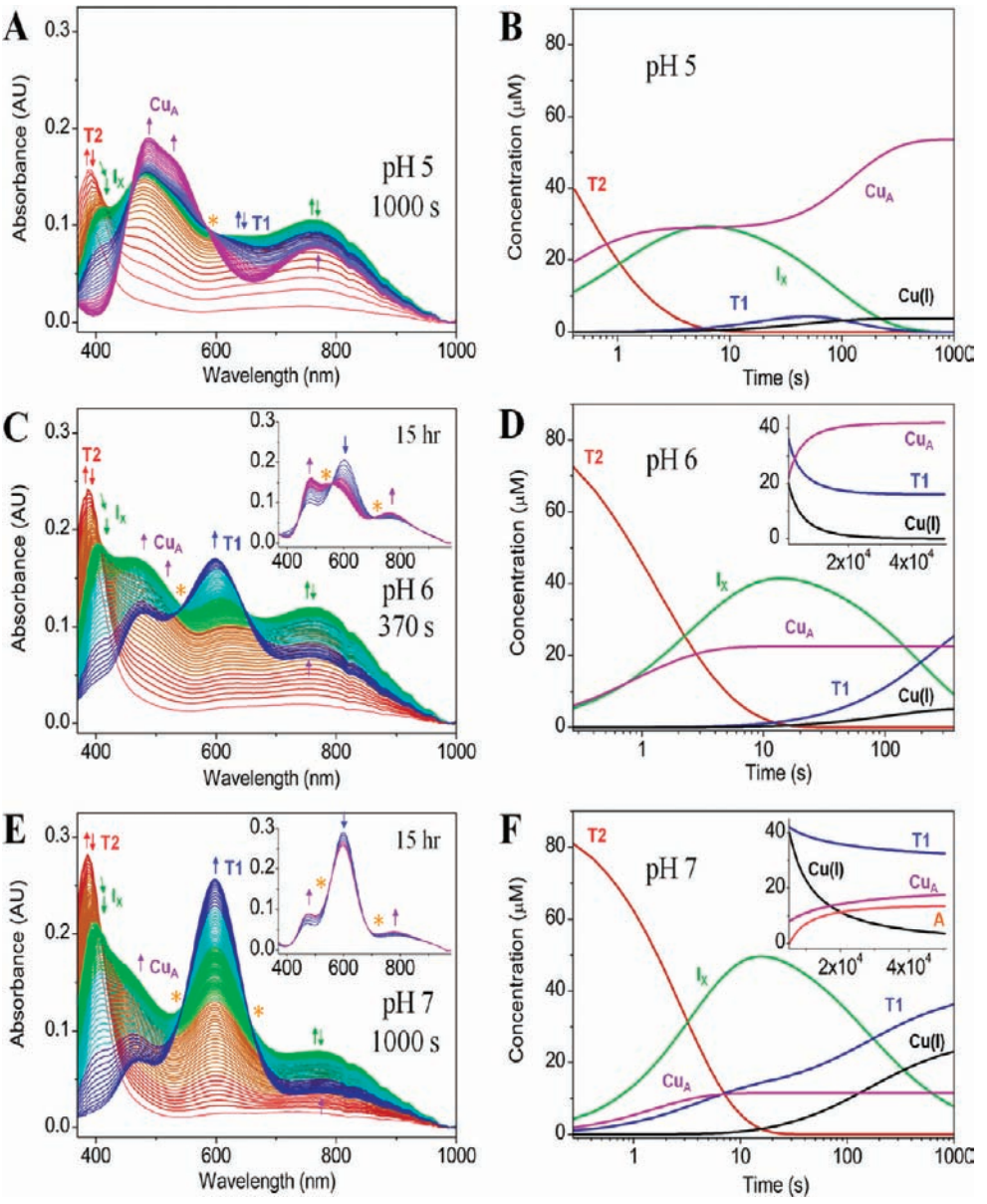

Figure 2. Stopped-flow UV−vis absorbance spectra (A, C, E) and corresponding concentration profiles (B, D, F) after mixing of subsaturating 0.4 equiv of $CuSO_4$ with Cu_AAz (A and B) over 1000 s at pH 5, (C and D) over 370 s at pH 6, and (E and F) over 1000 s at pH 7 in UB. Insets: UV−vis absorbance spectra (C, E) and corresponding concentration profiles (D, F) of subsequent overnight process (final time point: 15 h from $CuSO_4$ addition). Full data sets corresponding to the overnight processes in the insets can be found in Figure S21. (A, C, E) Spectra are colored to indicate the species forming at that particular time. Arrows indicate direction of change in absorbance over course of experiment and are colored to correspond to the species giving rise to that peak. Golden asterisks indicate the positions of apparent isosbestic points. Final Cu_AAz concentrations were 0.25 mM and $CuSO_4$ concentrations were 0.1 mM. Stopped-flow spectra were collected in each case with a logarithmic scale over 1000 s and 200 total spectra. The first spectrum was collected at 0.134 s. For the overnight UV−vis data collection, spectra were collected initially with a 0.5 s scan time, which was incremented by 5% after 45 s over 900 s (pH 6 and 7), to make sure that the initial portion of the data matched that collected on the stopped-flow instrument (Figure S21). The spectra shown in the insets were collected with a 600 s scan time, which was incremented by 1% after 3600 s over 50 400 s (14 h). An additional 2 h of spectra were collected at 600 s intervals in the case of the pH 7 set of data, to ensure that no further significant changes were occurring (data not shown). (B, D, F) Concentration profiles are those resulting from global analysis of the corresponding kinetics data. Further information about the global analysis process may be found in the Experimental Section about fitting of the kinetics data.

spectroscopy were similar to those at pH 5 (Figure 2C,D, Scheme 1). The step where I_X decayed and absorption in the ~620 nm region increased was, however, much more pronounced at pH 6 than at pH 5, culminating in a clearly defined peak with $\lambda_{max} \sim 600$ nm, typical of a T1 blue Cu center. This process also produced an isosbestic point at 540 nm between the spectrum of I_X and that of T1 Cu. At longer time scales, the spectrum of T1 blue Cu decayed and the final spectrum of Cu_A emerged, accompanied by isosbestic points at 550 and 700 nm, strongly suggesting conversion of the T1 blue Cu center to Cu_A (see inset of Figure 2C). In general, the maximum absorptions of the intermediates were greater at pH 6 than at pH 5 and the kinetic processes slower, with completion of Cu_A formation taking 15 h at pH 6 versus ~0.3 h at pH 5 (see Figure 2, Scheme 1).

dx.doi.org/10.1021/ja205281t |J. Am. Chem. Soc. 2011, 133, 20778–20792

Scheme 1. Summary of Species Observed by UV−Vis Absorption Spectroscopy and Models Yielding Optimal Fits for the Kinetics of pH-Dependent, Aerobic Copper Incorporation and Oxygen-Dependent, pH 5, Copper Incorporation into Cu_AAz[a]

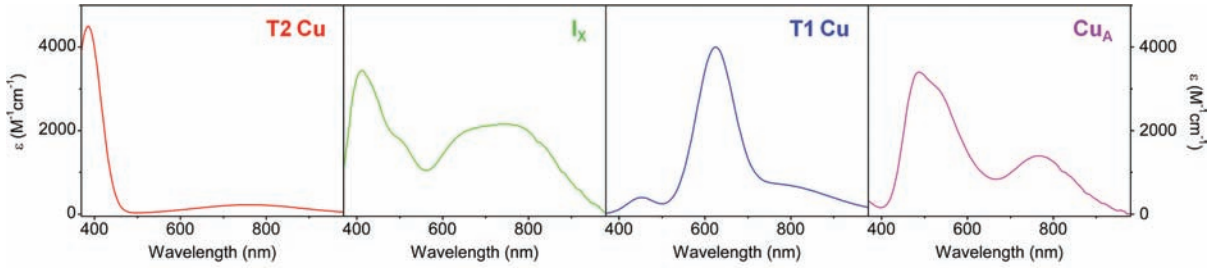

Summary of Models Yielding Optimal Fits for pH- and O_2-Dependent Kinetics of Cu_AAz upon Addition of $CuSO_4$

pH 5	$CuSO_4 \rightarrow T2$	$11.7 \pm 1.2\ s^{-1}$	Anaerobic	$15.1 \pm 1.2\ s^{-1}$
	$2\,T2 \rightarrow Cu_A$	$(12.9 \pm 0.52)\times10^{3}\ M^{-1}s^{-1}$		$(17.2 \pm 0.5) \times 10^{3}\ M^{-1}s^{-1}$
	$T2 \rightarrow I_X$	$0.460 \pm 0.034\ s^{-1}$		$0.854 \pm 0.022\ s^{-1}$
	$2\,I_X \rightarrow Cu(I)$	$82.2 \pm 11.9\ M^{-1}s^{-1}$		$48.5 \pm 0.9\ M^{-1}s^{-1}$
	$I_X \rightarrow T1$	$(7.93 \pm 0.40)\times10^{-3}\ s^{-1}$		$I_X + Cu(I) \rightarrow Cu_A$ $235 \pm 19\ M^{-1}s^{-1}$
	$T1 \rightarrow Cu_A$	$(3.37 \pm 0.03)\times10^{-2}\ s^{-1}$		
pH 6	$CuSO_4 \rightarrow T2$	$40.6 \pm 2.9\ s^{-1}$	Aerobic	$CuSO_4 \rightarrow T2$ $11.8 \pm 1.1\ s^{-1}$
	$2\,T2 \rightarrow Cu_A$	$(3.39 \pm 0.11)\times10^{3}\ M^{-1}s^{-1}$		$2\,T2 \rightarrow Cu_A$ $(13.2 \pm 1.1) \times 10^{3}\ M^{-1}s^{-1}$
	$T2 \rightarrow I_X$	$0.241 \pm 0.007\ s^{-1}$		$T2 \rightarrow I_X$ $0.831 \pm 0.031\ s^{-1}$
	$2\,I_X \rightarrow Cu(I)$	$25.6 \pm 1.0\ M^{-1}s^{-1}$		$2\,I_X \rightarrow Cu(I)$ $59.5 \pm 2.7\ M^{-1}s^{-1}$
	$I_X \rightarrow T1$	$(3.25 \pm 0.10)\times10^{-3}\ s^{-1}$		$I_X \rightarrow T1$ $(9.28 \pm 0.24) \times 10^{-4}\ s^{-1}$
	$T1 + Cu(I) \rightarrow Cu_A$	$6.99 \pm 0.36\ M^{-1}s^{-1}$		$T1 \rightarrow Cu_A$ $(1.63 \pm 0.11) \times 10^{-3}\ s^{-1}$
pH 7	$CuSO_4 \rightarrow T2$	$56.3 \pm 3.5\ s^{-1}$	O_2-Rich	$CuSO_4 \rightarrow T2$ $14.6 \pm 1.4\ s^{-1}$
	$2\,T2 \rightarrow Cu_A$	$(0.948 \pm 0.047)\times10^{3}\ M^{-1}s^{-1}$		$2\,T2 \rightarrow Cu_A$ $(10.5 \pm 1.3) \times 10^{3}\ M^{-1}s^{-1}$
	$T2 \rightarrow T1$	$(4.43 \pm 0.27)\times10^{-2}\ s^{-1}$		$T2 \rightarrow I_X$ $0.944 \pm 0.038\ s^{-1}$
	$T2 \rightarrow I_X$	$0.182 \pm 0.006\ s^{-1}$		$2\,I_X \rightarrow Cu(I)$ $60.4 \pm 2.7\ M^{-1}s^{-1}$
	$2\,I_X \rightarrow T1 + Cu(I)$	$55.7 \pm 2.8\ M^{-1}s^{-1}$		$I_X \rightarrow T1$ $(9.28 \pm 0.24) \times 10^{-4}\ s^{-1}$
	$T1 + Cu(I) \rightarrow Cu_A$	$0.521 \pm 0.023\ M^{-1}s^{-1}$		$T1 \rightarrow Cu_A$ $(1.58 \pm 0.09) \times 10^{-3}\ s^{-1}$
	[a] $2\,Cu(I) \rightarrow A$	1.60 (fixed) $M^{-1}s^{-1}$		

[a] The representative UV-Vis spectra are those resolved by the global analysis of the data from Cu_AAz at pH 5, with addition of 0.4 equivalents $CuSO_4$. [b] This step was not required in the model in order for the fit to converge, but improved the quality of the fit. The nature of the product A is not known, and so it is given a generic label here. The associated fixed rate was chosen based on the improvement to the fit. A wide range of values were explored before selecting the one given here.

The spectral changes and intermediate formation at pH 7 (Figure 2E,F) were broadly similar to those at pH 6, but with some differences. First, the kinetics of the intermediate and final Cu_A product formation were further slowed. Higher absorptions from the T2 Cu, I_X, and T1 Cu intermediates were also observed, including a significant contribution of the T1 blue Cu intermediate in the final spectrum collected at 15 h (Figure 2E plus inset). As a result, clearer isosbestic points at 554 and 681 nm between the spectrum of I_X and that of T1 Cu were observed, suggesting a clean conversion of I_X to the T1 Cu center. We performed the same experiment at pH 8, but instability of the protein and/or intermediates led to inconsistent results.

Time Dependent EPR Spectral Studies of Cu_AAz after Addition of a Subsaturating Amount of $CuSO_4$. To further characterize the intermediates over the course of copper incorporation, EPR spectra were collected at various times after adding a subsaturating amount of $CuSO_4$ (Figure 3, Table 1). A pH of 7 and 0.1 equiv of $CuSO_4$ were chosen for this set of experiments, since the rates of conversion of the intermediates were slower and greater accumulation of the intermediates occurred under these conditions, which made capture of all of the intermediates by EPR possible. An EPR sample of Cu_AAz, 100 ms after mixing with 0.1 equiv of $CuSO_4$, was prepared using a freeze quench apparatus, and the spectrum in Figure 3A was collected as a result. This spectrum was fit by a single species using EPR spectral simulation, and this species displayed $A_z = |147| \times 10^{-4}\ cm^{-1}$ (Table 1), typical of T2 Cu centers.[6] Stopped-flow UV−vis spectra collected under the same conditions of 10-fold excess protein indicated that the initial T2 Cu intermediate is maximized by 100 ms (Figure S22). Therefore, the species at 100 ms is assigned as the T2 Cu intermediate. Freeze quench samples prepared at 1, 5, and 10 s after $CuSO_4$ addition show the gradual decay of the T2 Cu species, and the growth of a new set of species, which is consistent with the time frame for the decay of the T2 Cu intermediate and with the subsequent 30 s spectrum (Figure S23).

Another sample of Cu_AAz was flash frozen 30 s after the addition of $CuSO_4$, and the EPR spectrum in Figure 3B was collected. UV−vis spectra collected for an identically prepared sample indicate that I_X and rapidly formed Cu_A (Cu_A') were present in this sample at 30 s (Figure S24). Thus, as expected, this early spectrum could not be assigned to a single Cu(II) species. EPR spectral simulation suggested the presence of one distinct species with a well-resolved axial spectrum, having small $g_z = 2.200$ and $A_z = |47| \times 10^{-4}\ cm^{-1}$ (Table 1). These parameters are similar to the published parameters for a mutant in which His120 is removed (H120A-Cu_AAz, Table 1),[67] leading to the assignment of this species as Cu_A', or fully reconstituted Cu_A lacking His120 coordination, formed rapidly from the T2 Cu intermediate. Because of the overlap of this rapidly formed Cu_A

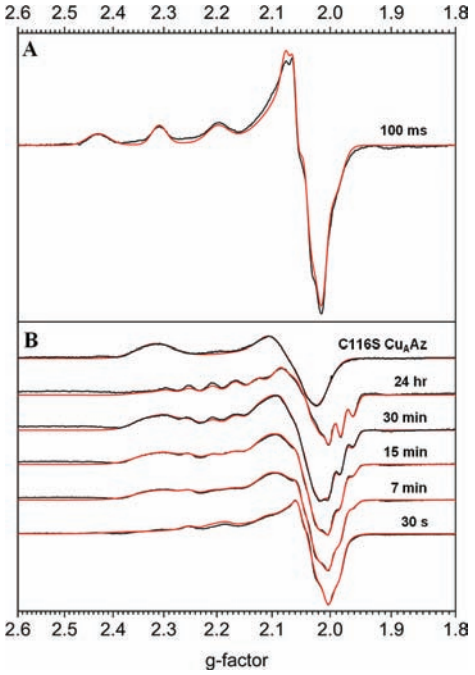

Figure 3. EPR spectra of Cu_AAz, pH 7 in TIP buffer, (A) at 100 ms and (B) at 30 s, 7 min, 15 min, 30 min, and 24 h after $CuSO_4$ addition, where the indicated times are incubation times at room temperature (20 °C, up to 30 min) or 4 °C (24 h sample). An EPR spectrum of C116S Cu_AAz, pH 7 in TIP buffer is shown for direct comparison. Black spectra are the experimental data, whereas red spectra are the corresponding simulated data. Concentration of the Cu_AAz sample is 4 mM, while the $CuSO_4$ concentration is 0.4 mM. For the C116S Cu_AAz sample, protein concentration is 2 mM and the $CuSO_4$ concentration, 0.5 mM. Approximately 10% (100 ms) and 30% glycerol is present in the samples, as a glassing agent. X-band experimental conditions: microwave frequency, 9.05 GHz; power, 0.2 mW (C116S), 0.5 mW (30s, 24 h), 1 mW (7, 15, and 30 min), 2 mW (100 ms); modulation amplitude, 2 G (C116S), 4 G (Cu_AAz); sweep time, 60s; gain, 6300 (30s, 24 h), 10 000 (100 ms, 7, 15, 30 min, C116S); temperature, 33 K. The spike at $g = 2.0$ is an artifact of the EPR tubes used.

with other species, Cu_A' and normal Cu_A (i.e., with His120 coordination) cannot be distinguished in the corresponding UV−vis spectrum.[74] For this reason, in the kinetic models of the UV−vis absorbance data, both Cu_A' and Cu_A were treated as a single species (Cu_A). This treatment is reasonable, because both species are Cu_A, just slightly different forms of it. As the changes in the absorptions of Cu_A upon protonation/deprotonation of His120 are minimal,[74] any error introduced as a result of this treatment is minor. In the 30 s spectrum, a second species was also observed, which simulation showed to have features intermediate between a T1 and T2 Cu complex, with $g_z = 2.234$ and $A_z = |115| \times 10^{-4}$ cm^{-1} (see Table 1). This species was tentatively assigned to I_X, as all other intermediates identified by electronic absorption spectroscopy were assigned, and the population of this species correlated well with that of I_X from UV−vis absorbance kinetics.

At 7 min after $CuSO_4$ addition, the signals that were dominant in the 30 s spectrum began to decay, and a species with $g_z \sim 2.31$ was observed, which gains intensity up to 30 min. The UV−vis spectra collected for an identically prepared sample show the absorbance band from the T1 blue Cu intermediate increases during this interval (Figure S24). Simulation of the EPR spectra containing this species found relatively large g-values ($g_x = 2.013$, $g_y = 2.063$, and $g_z = 2.307$) and small (unresolved) hyperfine splittings along all directions ($A_x = |24| \times 10^{-4}$ cm^{-1}, $A_y = A_z = |30| \times 10^{-4}$ cm^{-1}), as compared to typical copper complexes. This spectrum, which we assigned to the T1 blue Cu intermediate based on the parameters and the corresponding UV−vis spectra (Figures S8−S10, S12), was strikingly similar to the previously reported EPR spectrum of C116S Cu_AAz.[71] To gather further support for the EPR spectral similarity of the T1 blue Cu intermediate and C116S Cu_AAz, an EPR spectrum of the C116S variant of Cu_AAz was also collected under the same condition for direct comparison. As expected, the EPR spectrum of this C116S variant is almost identical to that of the third species recognized in the EPR spectra of Cu_A.

Meanwhile, starting at 7 min and continually increasing throughout the rest of the experiment, yet another species, with three hyperfine peaks visible between $g = 2.14$ and 2.27 and distinct features in the perpendicular range, became visible. From the nearly pure spectrum of this species, collected at 24 h after $CuSO_4$ addition, it was readily identified as Cu_A, as its parameters (Table 1) and seven-line hyperfine splitting pattern are almost identical to previous spectra.[61,67,74] The time frame for this process is also consistent with the UV−vis data collected under these conditions (Figure S24).

Oxygen-Dependent Copper Incorporation into Apo-Cu_AAz. Because of the reported involvement of molecular oxygen in the copper-catalyzed formation of disulfide bonds from thiols,[75−77] stopped-flow absorption spectral studies of Cu_AAz with $CuSO_4$ under anaerobic, aerobic, and oxygen-enriched conditions were conducted, to determine whether molecular oxygen played any role during the reconstitution of Cu_A. When Cu_AAz at pH 5 and a subsaturating 0.1 equiv of $CuSO_4$ were combined in the stopped-flow instrument under anaerobic, aerobic, and oxygen-enriched conditions, the absorption spectra in Figure 4 were observed over the subsequent 1000 s. Here, 0.1 equiv instead of 0.4 equiv of $CuSO_4$ was added, in order to further slow the kinetics and facilitate the observation of subtle differences in the formation of the intermediates. The initial $CuSO_4$ to T2 Cu step was too rapid to be characterized in the same set of data that was collected over 1000 s, so the kinetics of that step were fit separately, from the first several spectra of a data set collected over 50 s (Figure S25). The appearance and decay of the intermediates shown in Figure 4 and summarized in Scheme 1 were similar under all three conditions to what was observed in Figure 2A, with one key difference: the extent of formation of the ~620 nm peak, associated with the T1 blue Cu intermediate, correlates with the concentration of dissolved molecular oxygen.

UV−Vis Absorption Spectra of His120Ala Cu_AAz with Subsaturating Amounts of $CuSO_4$. To search protonatable ligands responsible for the pH-dependent copper incorporation into apo-Cu_AAz, pH-dependent UV−vis absorption spectra of H120A-Cu_AAz after addition of 0.1 equiv of $CuSO_4$ were collected (Figure 5). Previous studies have shown that the H120A-Cu_AAz variant displays a UV−vis spectrum similar to that of original Cu_AAz, despite the lack of one His ligand.[67,70] As compared to the spectral changes of original Cu_AAz, two major differences were readily observable for the H120A-Cu_AAz variant: the ~385 nm peak that formed initially and the ~600 nm peak that formed later in original Cu_AAz were both missing from the spectral changes in H120A-Cu_AAz, indicating absence of the T2 red and T1 blue Cu intermediates (for the complete set of spectra at each pH, see Figure S26). However, the ~400 and 750 nm bands of I_X still formed in H120A-Cu_AAz, and the

Table 1. EPR Parameters of the Species Identified through Simulation of Spectra in Figure 3 and the Various Percentages (±5%) of These Species as a Function of Time, As Determined from EPR Simulation

	T2 Cu	Cu_A'	I_X[a]	T1 Cu	Cu_A	C116S Cu_AAz	H120A Cu_AAz[b]
				Simulated Parameters of Species			
g_x	2.025	2.004	2.007	2.013	2.015	2.031	2.010
g_y	2.062	2.030	2.056	2.063	2.026	2.061	2.010
g_z	2.253	2.200	2.234	2.307	2.167	2.314	2.225
A_x (10^{-4} cm^{-1})	14	20	9	24	21 (Cu_1), 21 (Cu_2)	27	24 (Cu_1), 19 (Cu_2)
A_y (10^{-4} cm^{-1})	10	20	0.3	30	20 (Cu_1), 18 (Cu_2)	28	19 (Cu_1), 24 (Cu_2)
A_z (10^{-4} cm^{-1})	147	47	115	30	61 (Cu_1), 60 (Cu_2)	28	46 (Cu_1), 7 (Cu_2)
				Population of Species (%) at Time			
100 ms	100	0	0	0	0	-	-
30 s	0	40	55	5	0	-	-
7 min	0	20	20	50	10	-	-
15 min	0	10	15	60	15	-	-
30 min	0	0	0	75	25	-	-
24 h	0	0	0	30	75	-	-

[a] Tentative assignment. The percentage of this species correlates well with the kinetics of I_X in the electronic absorption spectra, and all other species have been identified. However, as a pure EPR spectrum of this intermediate has not yet been obtained, this assignment must remain tentative. [b] From ref 64.

shoulder at ~475 nm in the spectra of I_X appeared to correlate well with the amount of Cu_A formed under each condition (Figure 5), again suggesting that some Cu_A is rapidly formed; this observation was also consistent with the kinetic models used to fit the data in Figures 2 and 4. Another difference from original Cu_AAz is that little or no Cu_A appears to form after the initial, rapidly formed Cu_A. The presence of rapidly formed Cu_A suggests that the T2 red Cu intermediate still forms in the H120A mutant, making Cu_A through the 2 T2 → Cu_A pathway, and that this T2 Cu intermediate formed too quickly to be observed (i.e., formation of the T2 Cu intermediate was no longer a rate-determining step). This is reasonable, because His120 acts as a "gate" on the surface of the protein, excluding the Cu_A center from solvent.[67,74] The H120A mutation makes the site more accessible to copper, thus, accelerating T2 Cu and subsequent Cu_A formation. Additionally, these data demonstrated strong pH dependence for Cu_A site formation. At low pH (i.e., pH 5), substantial Cu_A formation was observed; however, as the pH was raised, the amount of Cu_A formed dropped off precipitously, with very little Cu_A formation seen at pH 7. Plotting the final absorbance at 485 nm against pH revealed a linear relationship between these parameters (see Figure S27).

DISCUSSION

Overall Kinetics of Copper Incorporation into Cu_AAz: Similarities to Cu_A in Native N_2OR. The Cu_AAz construct was designed as a biomimetic model of native Cu_A sites,[59] and several spectroscopic, X-ray crystallographic, and electron transfer studies have established that Cu_AAz is a close structural and functional model of these Cu_A centers.[13,19,61,63−67] In a previous study of the native Cu_A center in N_2OR,[33] we discovered that formation of the purple Cu_A center went through T2 red and T1 blue Cu intermediates, characterized by peaks at ~385 and 640 nm, respectively. From Figure 2 in this study, peaks at ~390 and 600 nm were observed to appear after addition of copper to apo-Cu_AAz before the final spectrum of purple Cu_A formed. Given the intensity of these absorption bands and their positions, the ~390 nm peak can be assigned as a T2 copper site with thiolate coordination (i.e., a red copper site, by analogy to the native T2 cupredoxin), while the ~600 nm peak falls into the classification of T1 blue Cu sites.[6,7] Although the λ_{max} of this T1 blue Cu intermediate differs by ~40 nm from that in N_2OR, this degree of variation is found among native T1 blue Cu proteins, and, despite this variation, the primary coordination spheres of all of these T1 blue copper sites are remarkably similar.[2,78] Thus, the difference in λ_{max} of the T1 blue Cu intermediate between N_2OR and Cu_AAz is not surprising, and these values are still indicative of similar sites between the two proteins. Not only are the T2 red and T1 blue Cu intermediates similar between Cu_AAz and N_2OR, these intermediates also show similar pH dependence in both proteins: greater accumulation of the intermediates relative to Cu_A as the pH increases (Figure 2 and ref 33). Therefore, the engineered Cu_AAz is an excellent model of native Cu_A centers, as it not only displays almost identical structural and functional properties, but its kinetics of copper incorporation also resemble those of the native Cu_A site of N_2OR. More importantly, the faster kinetics of copper incorporation into Cu_AAz relative to N_2OR allowed us to utilize lower copper equivalents, which mimics more closely the limited availability of copper ions in the cellular environment. These copper limiting conditions unveiled a pathway to copper incorporation involving a new intermediate (I_x). Furthermore, readily available variants of Cu_AAz, where the key Cys and His ligands are mutated, have enabled us to elucidate key ligands responsible for the formation of the intermediates.

Kinetics of Copper Incorporation in Cu_AAz under Copper Saturating versus Subsaturating Conditions: Differences from Cu_A in N_2OR. In the titrations of Cu_AAz with a saturating amount of $CuSO_4$ at pH 5, 6, and 7, whereas the T2 red and T1 blue Cu intermediates were observed similarly to those in N_2OR,[33] the T1 blue Cu intermediate decayed without an obvious isosbestic point to indicate conversion to the Cu_A site formed in the end (Figure S1). In contrast, when N_2OR was titrated with a similar saturating amount of $CuSO_4$, clear

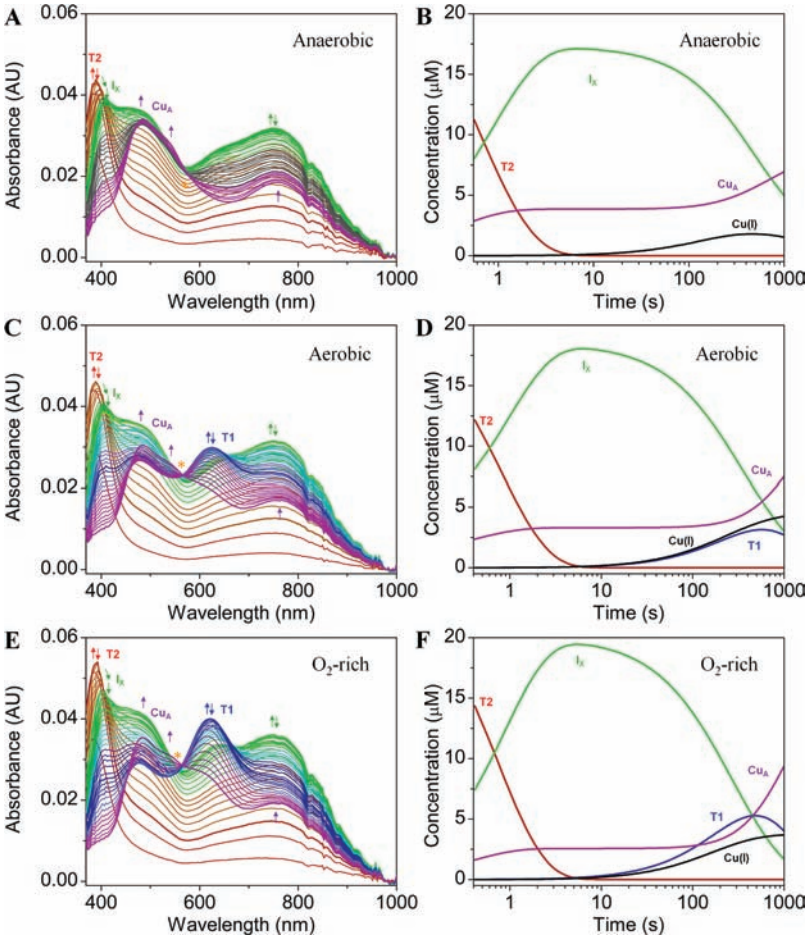

Figure 4. Stopped-flow UV−vis absorption (A, C, E) and concentration profiles (B, D, F) of Cu_AAz in 10-fold excess over $CuSO_4$ at pH 5 under (A and B) anaerobic, (C and D) aerobic, and (E and F) O_2-rich conditions. (A, C, E) Spectra are colored to indicate the species forming at that particular time. Arrows indicate direction of change in absorbance over course of experiment and are colored to correspond to the species giving rise to that peak. Golden asterisks indicate isosbestic points. Spectra (200 total) were collected in each case with logarithmic scale over 1000 s. Final protein concentration was 0.25 mM in 50 mM NaOAc, pH 5.0 ± 0.1, and $CuSO_4$, 0.025 mM. Average temperature was 16.1 °C. (B, D, F) Concentration profiles are those resulting from global analysis of the corresponding kinetics data. Further information about the global analysis process may be found in the Experimental Section about fitting of the kinetics data.

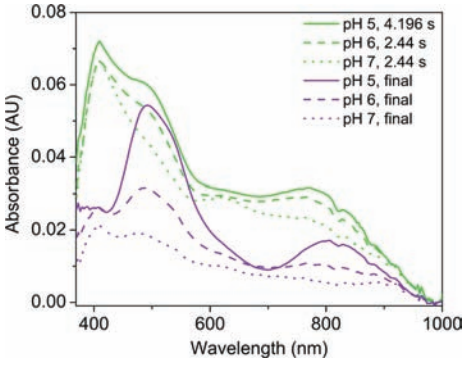

Figure 5. Representative UV−vis absorbance spectra of H120A Cu_AAz mixed with 0.1 mol equiv of $CuSO_4$, showing maximum I_X formation at 4.196 s for pH 5 and 2.44 s for pH 6 and 7. The final spectra after 1000 s are also shown for each pH. Final protein concentrations were 0.4 mM and $CuSO_4$ concentration was 0.035 mM. Average temperature was 16.3 °C.

isosbestic points were observed between the T1 blue Cu intermediate and Cu_A.[33] However, when subsaturating amounts of $CuSO_4$ were added to apo-Cu_AAz under otherwise identical conditions, isosbestic conversion of the T1 blue Cu species to Cu_A was unmistakable (Figure 2). We attribute the differences between these proteins to the fact that N_2OR is a much larger protein with a total of 10 cysteine residues, many of which are in close proximity to each other (PDB ID 1FWX),[79] and could serve as sacrificial reductants. In contrast, each molecule of Cu_AAz contains only four cysteine residues, two of which natively form a disulfide and the other two being Cys ligands in the Cu_A site (PDB ID 1CC3).[63] Since reducing equivalents are required to form the mixed valent $[Cu(1.5)\cdots Cu(1.5)]$ Cu_A center from $CuSO_4$, the Cys thiols in these proteins likely serve as sacrificial reductants, as proposed in previous reports on the reconstitution of both Cu_AAz[73] and N_2OR.[33] Because of the excess of free Cys residues in N_2OR capable of forming disulfide bonds, the reducing capacity per molecule of N_2OR is much greater than that per molecule of Cu_AAz. Accordingly, if the Cu_A sites were saturated with Cu(II), N_2OR could still provide reducing equivalents at a ratio of copper to protein equal or greater than one, resulting in the formation of more Cu_A sites in N_2OR. In the case where the Cu_A site of Cu_AAz is saturated with Cu(II), all of

the thiols are used up to form Cu_A, the various intermediates, or have already formed disulfide and Cu(I), and therefore are not available to provide further reducing equivalents. However, under subsaturating $CuSO_4$ conditions, not all of the thiols in the Cu_A site of Cu_AAz are occupied or disulfide-bonded, so these additional sites are able to provide reducing equivalents, permitting conversion of the T1 blue Cu species to Cu_A. Another influence of subsaturating $CuSO_4$ conditions that could lead to additional formation of Cu_A is that excess apo-Cu_AAz likely stabilizes the Cu(I) produced in situ—which is unstable in aqueous solution in the absence of coordinating small molecules or proteins—by binding to the Cys residues in the Cu_A site.

pH-Dependence of Copper Incorporation in Cu_AAz: Contributions from Redox Potential and His120. From the spectra in Figure 2 and the associated rates in Scheme 1, it can be seen that the copper incorporation into Cu_AAz is highly dependent on pH, with slower formation of the final Cu_A center and greater accumulation of the intermediates as the pH is raised from pH 5 to 7. One factor contributing to this observation is the known ubiquitous dependence of reduction potential upon pH exhibited by the copper sites of cupredoxin proteins; the redox potential of the copper site of *P. aeruginosa* Az decreases by ~60 mV as the pH is increased from 5.0 to 8.0.[80,81] This trend should generally apply to the copper intermediates observed here as well, since it was attributed to the protonation of two histidines, neither being copper ligands, and thus both intact in Cu_AAz. This trend was already shown to apply to the Cu_A site in Cu_AAz.[74] At low pH, therefore, we expect the reduction potential of the copper ion in the intermediates to be higher. Because reduction of Cu(II) to Cu(I) is an important step for the formation of the mixed valent $[Cu(1.5)\cdots Cu(1.5)]$ Cu_A site, the higher the driving force for the Cu(II)/Cu(I) redox couple, the faster the reduction may occur, increasing the availability of Cu(I) for forming the final product at low pH. As the pH is raised, the redox potential is lowered, making it more difficult to reduce Cu(II) to Cu(I), and decreasing the availability of Cu(I), which slows the final Cu_A formation and allows more accumulation of the intermediates.

Another factor contributing to the pH dependence of both intermediate and Cu_A formation in Cu_AAz is His120. H120A-Cu_AAz shows similar, but more drastic, pH dependence of Cu_A formation (Figure 5) to original Cu_AAz, with Cu_A formation dropping off linearly with pH (Figure S27). Therefore, an explanation for the observed pH-dependence of the rapidly formed Cu_A is that His120 is protonated and incapable of binding the copper at low pH. The EPR spectrum of Cu_AAz, pH 7, 30s after $CuSO_4$ addition and its simulated parameters (Figure 3, Table 1) provide support for this possibility. Here, the distinct species, Cu_A', identified through simulation has EPR parameters nearly identical to those previously reported for a species observed in low pH, His120-off holo-Cu_AAz and in holo-H120A Cu_AAz (Table 1).[67,74] Previous studies indicate that, when protonated, His120 in Cu_AAz swings away from the site, becoming more solvent exposed and creating an open coordination site.[67,74] Given that two coppers need to enter the site to form Cu_A, the loss of steric encumbrance from His120 may greatly expedite this process and thus yield faster rates of Cu_A formation at low pH. As the pH is raised, a greater portion of His120 is deprotonated in Cu_AAz, and therefore able to bind copper and slow down the Cu_A formation. Interestingly, no T2 Cu or T1 Cu intermediates were observed in the copper incorporation into the H120A-Cu_AAz (Figure 5), suggesting that His120 is essential for formation of these intermediates (vide infra).

Identity of the T2 Red and T1 Blue Cu Intermediates: EPR and Cys-Knockout Mutants Provide Clues. Because of the transient nature of the copper intermediates formed during reconstitution of Cu_AAz, and in many cases, their overlapping temporal existence, it is difficult to determine the characteristics of these copper sites. Fortunately, Cu(II) interactions with thiolate supply UV—vis handles, through monitoring of the S(Cys) → Cu(II) ligand-to-metal charge transfer (LMCT) bands. The molar absorptivity and energy of these LMCT transitions are diagnostic of the type of copper site involved.[6,7] The first species to appear, namely the ~385 nm peak, can be assigned to a tetragonal copper—thiolate center, similar to that found in the native T2 red Cu protein. The relatively large A_z of $|147| \times 10^{-4}$ cm^{-1} (Table 1) for this initial species is also consistent with its assignment as a T2 Cu intermediate. The species associated with the ~600 nm peak can be attributed to a distorted tetrahedral copper—thiolate center, analogous to those found in native T1 blue Cu proteins, where the EPR parameters of this species are also consistent with this assignment (Table 1).

An earlier study, in which each of the two active site Cys of Cu_AAz were, in turn, mutated to isostructural serine[71] (a residue that does not produce the same LMCT bands when interacting with copper) provided further insights into the makeup of these T2 red and T1 blue Cu intermediates. Notably, it was discovered that replacing Cys112 with Ser, leaving Cys116 intact to interact with Cu(II), resulted in a T2 red Cu complex with λ_{max} ~ 390 nm in its UV—vis spectrum.[71] The UV—vis spectrum of the copper-loaded C112S-Cu_AAz mutant is nearly identical to that observed for the T2 red Cu intermediate in original Cu_AAz observed in Figure 2. Conversely, replacing Cys116 with Ser, which only leaves Cys112 to interact with Cu(II), yielded a T1 blue Cu complex.[71] The EPR and UV—vis spectra of both the T1 blue Cu intermediate observed here during Cu_A formation in original Cu_AAz and the T1 blue Cu site formed in C116S-Cu_AAz are markedly similar (Figure 3 and Figures S8—S10, S12).[71] Therefore, the evidence suggests that the T2 red Cu intermediate in Cu_AAz arises from a complex with Cys116, while the T1 blue Cu intermediate results from a complex with Cys112. This conclusion is supported by the difference in accessibility of Cys112 and Cys116 to exterior Cu(II) ions. From the crystal structure of Cu_AAz (PDB ID: 1CC3), Cys116 is revealed to be closer to the surface of the protein than Cys112, rendering it free to capture Cu(II) from solution and form the T2 Cu center first, which then undergoes conformational rearrangement, leading to I_X (vide infra). Unlike the native T2 red Cu protein, nitrosocyanin, no evidence of superhyperfine splitting from histidine coordination could be detected in the perpendicular region of the T2 Cu species' EPR spectrum (Figure 3A), consistent with the hypothesis that this species is a capture complex with Cys116. On the basis of the UV—vis spectra of H120A-Cu_AAz in Figure 5, removal of His120 changes this situation; instead of the T2 red Cu intermediate forming and then decaying to I_X and Cu_A', I_X and Cu_A' form directly. Thus, His120 may be forcing Cys116 sterically or through hydrogen bonding interactions to orient toward the exterior of the protein. Because the T1 blue Cu intermediate forms from oxidation of the reduced copper product of I_X decay, its absence from the spectra of H120A Cu_AAz suggests that His120: (1) is a required ligand in the T1 blue Cu species; (2) lowers the reduction potential of the Cu(I) precursor to the T1 Cu species, making this species more accessible

Scheme 2. Current Picture of How Cu(II) Is Incorporated into the Cu_A site[a]

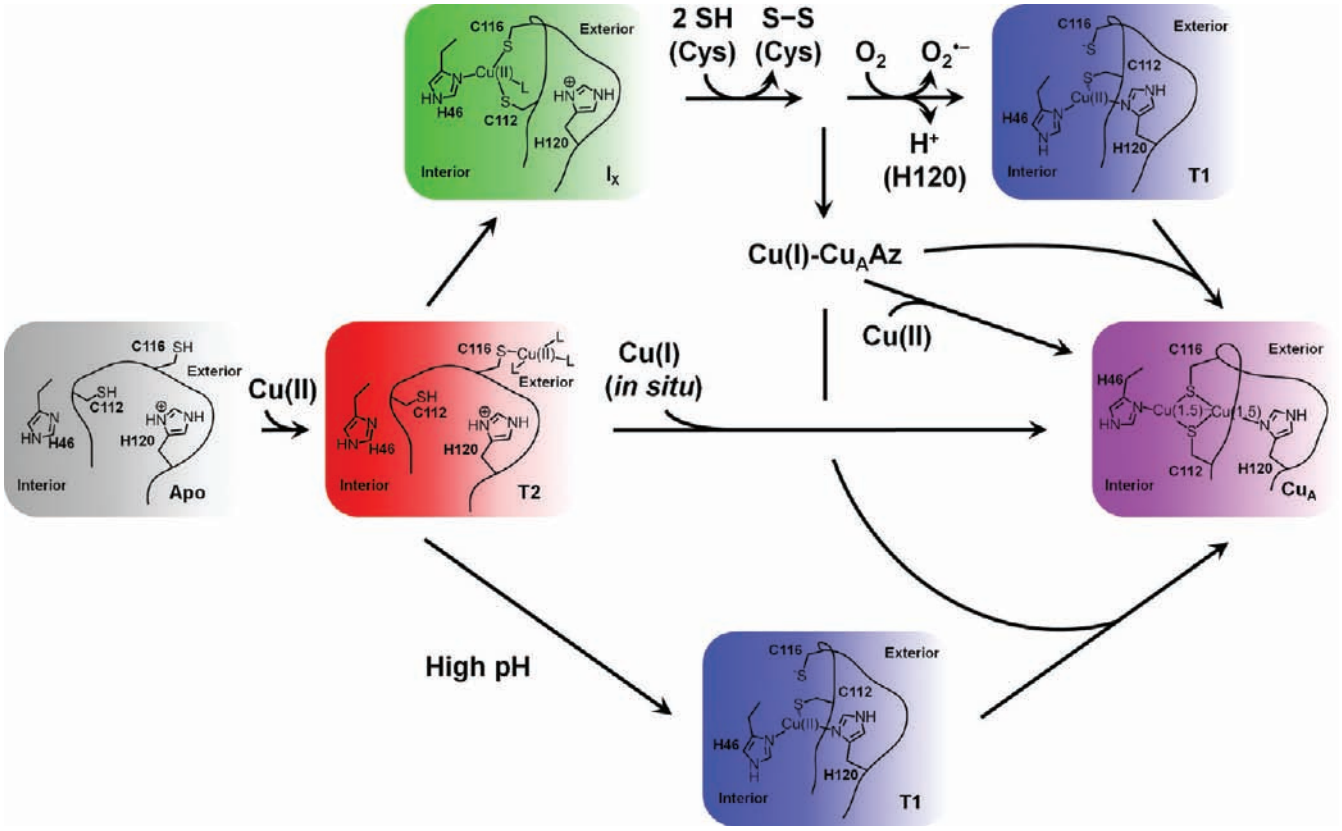

[a] Interior and exterior labels are used to indicate the inside versus the outside of the protein.

to oxidation by O_2; or (3) is required to protect the Cu(I) precursor to the T1 Cu species from bulk solution. While we have not eliminated the latter two possibilities, given the highly conserved, His-Cys-His primary coordination sphere of native T1 blue Cu sites, the first possibility is most likely. In support of His120 being a required ligand for the formation of the T1 Cu intermediate, the pH dependence of the T1 blue Cu intermediate formation in Cu_AAz (Figure 2) falls into a similar range as the determined pK_a of His120.[74]

Identity of I_X: Its Instability with Respect to Reduction and Unusual Spectral Properties. A particularly interesting discovery of this study is that of I_X, having intense absorptions at 410 and 760 nm that are not immediately diagnostic of any known copper−thiolate binding site. Like the T1 blue Cu intermediate, I_X was not observed in the previous study of copper incorporation into the Cu_A site of Cu_AAz.[73] In the previous study, where 10-fold excess copper over protein conditions were used, the only process observed was the direct formation of Cu_A from the T2 red Cu intermediate.[73] This result makes sense from the observed rate constants and kinetics fits for copper incorporation in the present study, as the direct T2 to Cu_A pathway is bimolecular with respect to the T2 intermediate with a large observed rate constant (Scheme 1). Thus, at greater concentrations of copper, where more T2 red Cu intermediate forms, this step dominates the copper incorporation process.

In the present study, subsaturating amounts of copper were used, and insufficient T2 Cu was formed to completely support the bimolecular direct T2 to Cu_A pathway. As a result, a slower step, where T2 is converted to I_X, competes for the initial pool of T2 Cu. The slower rate of the T2 to I_X step (Scheme 1) indicates that this step is accompanied by structural rearrangement of the T2 red Cu site, such as ligation of another residue from the protein to the copper. As discussed above, the T2 red Cu site is most likely a capture complex with a solvent-exposed Cys116. Thus, a picture emerges of the T2 red Cu capture complex swinging into the interior of the protein, perhaps being driven or accompanied by ligation of another residue (Scheme 2).

Once I_X is formed in Cu_AAz, it decays at similar rate regardless of changes to pH or O_2 content (Scheme 1). Likewise, the I_X that forms in H120A-Cu_AAz decays in the same time frame (nearly complete 1000 s after $CuSO_4$ addition). Under most conditions explored here, the decay of I_X is accompanied by formation of the T1 blue Cu intermediate (Figures 2 and 4). However, in the absence of molecular oxygen, although I_X decays at about the same rate (Figure 4, Scheme 1), its decay does not appear to correspond to the production of any colored species, highlighting the possibility that I_X is generating Cu(I) in this system. This hypothesis was confirmed by spin-quantification EPR, performed under the same conditions as in Figure 3, which shows loss of spin from the system over the same time frame that I_X is decaying (Figure S28). Thus, the loss of the I_X signal is associated with production of Cu(I). Incorporating this knowledge into the models used for fitting the copper incorporation kinetics resulted in high quality fits (Scheme 1, Tables S1 and S2, Figurea S14−S16 and S18).

Inferring the ligands and geometry of I_X is complicated by the fact that it is always present as one component in a mixture of several species. For this reason, the pure I_X UV−vis absorbance

and EPR spectra remain elusive. The resolved molar absorptivity spectra for I_X produced by the kinetics fitting procedure provide indications of the pure spectrum, and thus the identity of I_X (Figures S8−S10 and S12), as do the EPR parameters assigned to I_X (Table 1). In searching similar spectra to that of I_X from known Cu(II)−thiolate complexes, we found only one example: copper-substituted horse liver alcohol dehydrogenase (HLADH).[82] The electronic absorption spectra of copper-substituted HLADH in complex with exogenous ligands, including pyrazole and a coenzyme (modified nicotinamide adenine dinucleotide, H_2NADH), show similarly intense and broad transitions at low energy (690−720 nm versus ∼710−740 nm for I_X spectra in Figures S8−S10, S12), as well as intense transitions around 400 nm.[82,83] The copper center in these Cu(II)−HLADH complexes with exogenous ligands were interpreted and later confirmed to be distorted (flattened) tetrahedral copper dithiolate sites, consisting of Cu(II)−S_2(Cys)N(His)L (L = exogenous ligand, e.g., water, pyrazole, imidazole, 2-mercaptoethanol, etc.).[82,83] The tentatively assigned A_z of $|115| \times 10^{-4}$ cm^{-1} for I_X falls into an intermediate range for those typical of T1 and T2 Cu sites. However, this A_z is identical to that found for the binary complex of Cu(II)−HLADH with pyrazole,[84] and also similar to those of the complexes with imidazole and 2-mercaptoethanol.[85] Moreover, these complexes of Cu(II)−HLADH with pyrazole, imidazole, and 2-mercaptoethanol were metastable, bleaching over time, which was attributed to intramolecular reduction of the active-site Cu(II) to Cu(I) by the coordinated cysteine thiolates, presumably accompanied by formation of a disulfide.[84,85] This instability with respect to autoreduction is consistent with the behavior of I_X, as demonstrated by spin quantification EPR (Figure S28). On the basis of these results, we can deduce that I_X is formed from a rearrangement of the Cu(II)−Cys116 capture complex (i.e., T2 red Cu intermediate) into a Cu(II)−dithiolate complex, wherein Cys112 is the second thiolate ligand. Examples of other Cu(II)−dithiolate complexes for comparison to I_X are rare, as the thiol-ligands must have features that avoid the Cu(II)-catalyzed formation of disulfide from thiols.[75−77]

Oxygen-Dependence of the T1 Blue Cu Species: One-Electron Oxidation of the Cu(I) Product of I_X Decay. When oxygen was excluded from the reconstitution of Cu_AAz at pH 5, the T1 blue Cu species no longer formed (Figure 4). Conversely, when the reactant solution was enriched in O_2, more T1 blue Cu species formed than when the reactants were simply exposed to air (Figure 4). Thus, the extent of T1 blue Cu species formed correlates positively with the concentration of dissolved molecular oxygen in the reaction mixture. Since the T1 blue Cu intermediate is primarily the product of I_X, the key to understanding this oxygen-dependence may lie in examination of I_X. As discussed above, EPR spin-counting experiments connected the decay of I_X with the formation of Cu(I). The O_2-dependent stopped-flow UV−vis spectra are also consistent with this finding (Figure 4 and Scheme 1). The rates for the steps prior to the decay of I_X are similar regardless of the O_2 concentration and whether the T1 blue Cu intermediate forms. The amount of I_X remaining at the end of the 1000 s experiments is also nearly identical between anaerobic, aerobic, and O_2-rich conditions (Figure 4). Since I_X decays at about the same rate, regardless of whether the T1 blue Cu intermediate forms afterward, it is likely that the product of I_X decay is the same whether the T1 blue Cu intermediate subsequently forms. By extension, the T1 blue Cu intermediate formed after I_X is actually the product of a Cu(I) species, generated by the decay of I_X. Given that molecular oxygen must be present for this Cu(I) → T1 Cu transformation to occur, oxygen is presumably acting as an oxidant to the Cu(I) species. Therefore, the most likely mechanism leading to the observed oxygen-dependent formation of the T1 blue Cu intermediate is the formation of a reduced T1 blue Cu site, which then undergoes a one-electron oxidation to the T1 blue Cu intermediate, with oxygen serving as the oxidant.

Mechanism of Cu(II) Incorporation into the Cu_A Site. From all of these various data, a mechanistic picture begins to emerge (Scheme 2). Starting with apoCu_AAz and adding Cu(II), T2 red Cu formation occurs rapidly, as previously reported.[73] The UV-vis and EPR spectroscopic evidence for Cu_AAz and its Cys112Ser mutant (see Figure 3 and Figures S8-S10, S12) are consistent with the formation of a Cu(II) capture complex with Cys116. From the T2 red Cu intermediate, there are three pathways, all leading to purple Cu_A in the end. One pathway, reported in a prior study,[73] leads directly to purple Cu_A formation, presumably by the generation of Cu(I) ions *in situ* through the reaction of Cu(II) with an empty Cu_A site's thiolates to form a disulfide and Cu(I). In the presence of excess copper, this route is accelerated greatly and dominates the mechanism. This copper dependence suggests that the initial reductive event requires multiple coppers per Cu_A site, or multiple singly copper loaded proteins to interact and provide reducing equivalents, which is consistent with the 2 e^- reduction of thiols to disulfide. Conversely, the observed intermediates that form from I_X under subsaturating copper conditions are a result of single copper occupation of the Cu_A site. On the pathway that predominates at low copper concentration, the T2 red Cu center converts to I_X, likely through a structural rearrangement to a dithiolate complex. After formation of I_X, it decays, due to reduction of the copper to Cu(I) by the active site cysteine thiolates. Given the highly thiophilic nature of Cu(I), the Cu(I) generated likely binds to the free cysteines of another equivalent of apo-Cu_AAz, which is in strong excess. Some portion of this Cu(I) likely forms the reduced version of the Cu_A site, which can then be oxidized to the purple, [Cu(1.5)···Cu(1.5] state either by another Cu(II) site or by molecular oxygen.

All of the wt Cu_AAz electronic absorption studies (Figures 2 and 4) indicate that the next step is formation of the T1 blue Cu species when oxygen is present. UV-vis and EPR spectral evidence point to Cys112 coordination in the T1 Cu intermediate. Because no T1 blue Cu intermediate was observed in the UV−vis spectra of H120A-Cu_AAz (see Figure 5, Figure S26), His120 is required to form the T1 blue Cu species. Moreover, the pH-dependent UV−vis spectra (Figure 2) indicated that more T1 blue Cu species formed at higher pH. Given these observations and the fact that the His-Cys-His primary coordination sphere is completely conserved among T1 blue Cu sites, we can infer that deprotonation and coordination of His120 is a necessary step to formation of the T1 blue Cu intermediate. The other pathway from the T2 red Cu species supports this deprotonation step as well; in this pathway, the T1 blue Cu intermediate is formed directly from T2 Cu at high pH, where we would expect His120 to be deprotonated (see Figure 2E,F). Anaerobic and oxygen-rich stopped-flow data of Cu_AAz with $CuSO_4$ (Figure 4) also reveal that formation of the T1 blue Cu intermediate is dependent upon the concentration of molecular oxygen in solution, strongly suggesting one-electron oxidation of a Cu(I) precursor. Finally, isosbestic conversion of the T1 blue Cu intermediate to Cu_A occurs under subsaturating $CuSO_4$ conditions. On the basis of comparison to the native N_2OR

system (vide supra), it is inferred that reducing equivalents, that is, generation of Cu(I), are required to achieve this transformation. This scheme represents our current understanding of how Cu(II) leads to the formation of Cu_A in Cu_AAz under subsaturating copper conditions.

CONCLUSIONS

In this study, the kinetics of copper incorporation into the Cu_A site of an engineered structural and functional Cu_A model protein, Cu_AAz, have been characterized extensively by electronic absorption and electron paramagnetic resonance spectroscopies. These characterizations have provided new insight into the mechanism of Cu_A formation. It was found that, in addition to the previously discovered rapid T2 red Cu formation and conversion to Cu_A,[73] another pathway to Cu_A formation exists in Cu_AAz at lower copper equivalents, a condition that more realistically mimics the copper-limiting environment in vivo. From the T2 red Cu intermediate, conversion occurs to an intermediate, I_X, with unusual electronic absorption and EPR spectra, similar to those of a Cu(II)−dithiolate center.[82−85] I_X then decays to a Cu(I) species, where this step can be attributed to the Cu(II)-catalyzed formation of a disulfide bond between the cysteine thiols in the Cu_A site. Depending upon the protonation state, and the resulting ability to coordinate copper, of one of the active site histidines, molecular oxygen can then oxidize a Cu(I) site to a T1 blue Cu intermediate. Gradually, this T1 blue Cu intermediate isosbestically converts to the final purple Cu_A center. The observation of T1 blue and T2 red copper intermediates in the existing ligand set of now two Cu_A sites, both the native N_2OR protein[33] and biomimetic Cu_AAz model protein, suggests that the relationship among these three types of copper sites is universal and that the ligand loop is mainly responsible for the formation of the intermediates and final Cu_A center.

While the in vivo metalation of Cu_A sites is not completely understood, recent evidence suggests that the Cu(II) oxidation state is critical to the correct formation of this site in C*c*O.[37,86] Additionally, the Cu(II) oxidation state is stable in many environments in which Cu_A sites are found (e.g., bacterial C*c*Os[10,34,35] and N_2OR[36]).[87] Studies of the in vitro reconstitution of Cu_A sites with Cu(II) may provide valuable insight into the practicality of Cu(II)-driven metalation of Cu_A sites in vivo. This study demonstrates that Cu(II) reconstitution of Cu_AAz occurs through a complex multistep reaction, resulting in Cu_A sites, but the overall yield of this process is rather low, saturating at ∼30% of the total expected copper loading. Using a mixture of Cu(I) and Cu(II) yielded ∼20% more Cu_A sites than when Cu(II) alone was added (Figure S19). As the resting state of Cu_A requires a 1:1 ratio of Cu(I)/Cu(II), and the reducing equivalents to generate Cu(I) are provided by the active site Cys thiols when Cu(II) alone is used, it is not surprising that including Cu(I) in the reconstitution mixture improved the yield of Cu_A sites. Taken altogether, it is unlikely that the in vivo metalation of Cu_A relies solely on Cu(II). Instead, the use of a mixture of Cu(II) and Cu(I) is more likely in vivo. One can imagine that, in a controlled cellular setting, where a single molecule of C*c*O is metalated by individual chaperones, a concerted delivery of Cu(II) and Cu(I) may result in nearly 100% efficiency of Cu_A formation.

Now that the mechanism of Cu(II) incorporation into the Cu_A site of Cu_AAz is elucidated, the utility of thiol:disulfide oxidoreductases and copper chaperones in native systems becomes evident. The combination of a redox active metal (copper) with redox active ligands (cysteines) requires particularly expert handling. Direct incorporation of Cu(II), requiring reducing equivalents to fully form the Cu_A site, would greatly increase the likelihood of oxidative damage to the protein and inactivation of the electron transfer site. Yet, the unique and desirable properties of the Cu−S bond are such that nature has taken on the challenge, despite the risks.[88] Cu_A is the perfect embodiment of this dilemma: its unique structure makes it exceptionally well-suited to its task of electron transfer,[62,89] yet constructing the site without oxidizing cysteine and ejecting biologically toxic Cu(I) is particularly complex. Thus, this study demonstrates the extreme case of absent cellular management of copper, in relatively oxidizing cellular environments, such as in the periplasm and inner mitochondrial space,[90] where N_2OR and subunit II of C*c*O are found. Saturation of Cu_AAz at ∼30% of the total expected copper loading shows just how detrimental the use of the active site cysteines as reducing equivalents is to the system as a whole. It would be a tremendous waste of energy if 70% of cellularly synthesized metalloproteins were discarded due to misincorporation.

Nature has found a solution, though, for this quandary, as ubiquitous thiol:disulfide oxidoreductases are tasked with maintaining the proper oxidation state of cysteine residues. Such a role has been verified in vitro for the accessory protein Sco1 in *Thermus thermophilus* ba_3 oxidase in maintaining the active site cysteines of the Cu_A domain in the reduced state.[91] However, even if the formation of a disulfide in the active site is not itself an insurmountable problem, the other product of this reaction, Cu(I), can generate deleterious reactive oxygen species through Fenton-type chemistry if left unmanaged in the cell. Hence, nature utilizes copper chaperones, proteins specifically appointed to carry Cu(I) safely about the cell and deliver it to its target protein.[92] Thus, while functional Cu_A sites can indeed form from the addition of Cu(II) alone, nature's avoidance of this seemingly direct approach is well-justified.

ASSOCIATED CONTENT

Supporting Information. Tables and figures displaying parameters and results of global kinetics fits of UV−vis spectra, some additional discussions of the global kinetics fitting procedure. Figures of various titrations of apoCu_AAz with copper. Full sets of electronic absorption spectra for overnight kinetics experiments. Electronic absorption spectra corresponding to conditions under which EPR spectra were collected. Full sets of stopped-flow electronic absorption spectra for the H120A Cu_AAz mutant, a plot of the correlation between Abs(485 nm) and pH in this mutant. Plots of spin quantification and associated EPR spectra and $CuSO_4$ calibration. These materials are available free of charge via the Internet at http://pubs.acs.org.

AUTHOR INFORMATION

Corresponding Author
yi-lu@illinois.edu

ACKNOWLEDGMENT

The authors wish to thank Professor Robert Gennis for the use of his stopped-flow UV−vis instrument and Professor Wilfred A. van der Donk for the use of his freeze quench instrument; Igor Petrik, Shiliang Tian, and Kyle Miner for technical assistance; Dr.

Arnab Mukherjee for helpful discussions; and Niloufar Hafezi and Tim Mullen for general assistance. This material is based upon work supported by the National Science Foundation CHE 1058959.

REFERENCES

(1) Adman, E. T. *Adv. Protein Chem.* **1991**, *42*, 145.
(2) Gray, H. B.; Malmström, B. G.; Williams, R. J. P. *J. Biol. Inorg. Chem.* **2000**, *5*, 551.
(3) Solomon, E. I.; Randall, D. W.; Glaser, T. *Coord. Chem. Rev.* **2000**, *200*−*202*, 595.
(4) Vila, A. J.; Fernández, C. O. Copper in Electron Transfer Proteins. In *Handbook on Metalloproteins*; Bertini, I., Sigel, A., Sigel, H., Eds.; Marcel Dekker: New York, NY, 2001; pp 813.
(5) Solomon, E. I.; Szilagyi, R. K.; DeBeer George, S.; Basumallick, L. *Chem. Rev.* **2004**, *104*, 419.
(6) Lu, Y. Electron transfer: Cupredoxins. In *Biocoordination Chemistry*; Que, J. L., Tolman, W. B., Eds.; Elsevier: Oxford, U.K., 2004; Vol. 8, pp 91−122.
(7) Dennison, C. *Coord. Chem. Rev.* **2005**, *249*, 3025.
(8) Farver, O.; Pecht, I. *Prog. Inorg. Chem.* **2007**, *55*, 1.
(9) Blackburn, N. J.; Barr, M. E.; Woodruff, W. H.; van der Oost, J.; de Vries, S. *Biochemistry* **1994**, *33*, 10401.
(10) Iwata, S.; Ostermeier, C.; Ludwig, B.; Michel, H. *Nature* **1995**, *376*, 660.
(11) Tsukihara, T.; Aoyama, H.; Yamashita, E.; Tomizaki, T.; Yamaguchi, H.; Shinzawa-Itoh, K.; Nakashima, R.; Yaono, R.; Yoshikawa, S. *Science* **1995**, *269*, 1069.
(12) Henkel, G.; Müller, A.; Weissgräber, S.; Buse, G.; Soulimane, T.; Steffens, G. C. M.; Nolting, H. F. *Angew. Chem., Int. Ed.* **1995**, *34*, 1488.
(13) Andrew, C. R.; Lappalainen, P.; Saraste, M.; Hay, M. T.; Lu, Y.; Dennison, C.; Canters, G. W.; Fee, J. A.; Slutter, C. E.; Nakamura, N.; Sanders-Loehr, J. *J. Am. Chem. Soc.* **1995**, *117*, 10759.
(14) Brown, K.; Tegoni, M.; Prudencio, M.; Pereira, A. S.; Besson, S.; Moura, J. J.; Moura, I.; Cambillau, C. *Nat. Struct. Biol.* **2000**, *7*, 191.
(15) Haltia, T.; Brown, K.; Tegoni, M.; Cambillau, C.; Saraste, M.; Mattila, K.; Djinovic-Carugo, K. *Biochem. J.* **2003**, *369*, 77.
(16) Immoos, C.; Hill, M. G.; Sanders, D.; Fee, J. A.; Slutter, C. E.; Richards, J. H.; Gray, H. B. *J. Biol. Inorg. Chem.* **1996**, *1*, 529.
(17) Bertini, I.; Bren, K. L.; Clemente, A.; Fee, J. A.; Gray, H. B.; Luchinat, C.; Malmström, B. G.; Richards, J. H.; Sanders, D.; Slutter, C. E. *J. Am. Chem. Soc.* **1996**, *118*, 11658.
(18) Dennison, C.; Berg, A.; de Vries, S.; Canters, G. W. *FEBS Lett.* **1996**, *394*, 340.
(19) Gamelin, D. R.; Randall, D. W.; Hay, M. T.; Houser, R. P.; Mulder, T. C.; Canters, G. W.; de Vries, S.; Tolman, W. B.; Lu, Y.; Solomon, E. I. *J. Am. Chem. Soc.* **1998**, *120*, 5246.
(20) Antholine, W. E.; Kastrau, D. H. W.; Steffens, G. C. M.; Buse, G.; Zumft, W. G.; Kroneck, P. M. H. *Eur. J. Biochem.* **1992**, *209*, 875.
(21) Kroneck, P. M. H.; Antholine, W. E.; Koteich, H.; Kastrau, D. H. W.; Neese, F.; Zumft, W. G. *Bioinorg. Chem. Copper* **1993**, 419.
(22) Neese, F.; Zumft, W. G.; Antholine, W. E.; Kroneck, P. M. H. *J. Am. Chem. Soc.* **1996**, *118*, 8692.
(23) Farrar, J. A.; Neese, F.; Lappalainen, P.; Kroneck, P. M. H.; Saraste, M.; Zumft, W. G.; Thomson, A. J. *J. Am. Chem. Soc.* **1996**, *118*, 11501.
(24) Olsson, M. H. M.; Ryde, U. *J. Am. Chem. Soc.* **2001**, *123*, 7866.
(25) Abriata, L. A.; Ledesma, G. N.; Pierattelli, R.; Vila, A. J. *J. Am. Chem. Soc.* **2009**, *131*, 1939.
(26) Solomon, E. I. *Inorg. Chem.* **2006**, *45*, 8012.
(27) Lieberman, R. L.; Arciero, D. M.; Hooper, A. B.; Rosenzweig, A. C. *Biochemistry* **2001**, *40*, 5674.
(28) Savelieff, M. G.; Lu, Y. *J. Biol. Inorg. Chem.* **2010**, *15*, 461.
(29) Humphrey, W.; Dalke, A.; Schulten, K. *J. Mol. Graphics* **1996**, *14*, 33.
(30) Roberts, E.; Eargle, J.; Wright, D.; Luthey-Schulten, Z. *BMC Bioinf.* **2006**, *7*, 382.
(31) Ryden, L. G.; Hunt, L. T. *J. Mol. Evol.* **1993**, *36*, 41.
(32) Abolmaali, B.; Taylor, H. V.; Weser, U. *Struct. Bond.* **1998**, *91*, 91.
(33) Savelieff, M. G.; Wilson, T. D.; Elias, Y.; Nilges, M. J.; Garner, D. K.; Lu, Y. *Proc. Natl. Acad. Sci. U.S.A.* **2008**, *105*, 7919.
(34) Ostermeier, C.; Iwata, S.; Ludwig, B.; Michel, H. *Nat. Struct. Biol.* **1995**, *2*, 842.
(35) Soulimane, T.; Buse, G.; Bourenkov, G. P.; Bartunik, H. D.; Huber, R.; Than, M. E. *EMBO J.* **2000**, *19*, 1766.
(36) Zumft, W. G. *Microbiol. Mol. Biol. Rev.* **1997**, *61*, 533.
(37) Siluvai, G. S.; Nakano, M.; Mayfield, M.; Blackburn, N. J. *J. Biol. Inorg. Chem.* **2011**, *16*, 285.
(38) Ostermeier, C.; Michel, H. *Transition Met. Microb. Metab.* **1997**, 311.
(39) Komorowski, L.; Verheyen, W.; Schafer, G. *Biol. Chem.* **2002**, *383*, 1791.
(40) Suharti, M. J. F. S.; Schroeder, I.; de Vries, S. *Biochemistry* **2001**, *40*, 2632.
(41) Suharti, H. A. H.; de Vries, S. *Biochemistry* **2004**, *43*, 13487.
(42) Malmström, B. G.; Aasa, R. *FEBS Lett.* **1993**, *325*, 49.
(43) Lappalainen, P.; Saraste, M. *Biochim. Biophys. Acta Bioenerg.* **1994**, *1187*, 222.
(44) Bertagnolli, H.; Kaim, W. *Angew. Chem., Int. Ed.* **1995**, *34*, 771.
(45) Dennison, C.; Canters, G. W. *J. R. Neth. Chem. Soc.* **1996**, *115*, 345.
(46) Beinert, H. *Eur. J. Biochem.* **1997**, *245*, 521.
(47) Randall, D. W.; Gamelin, D. R.; LaCroix, L. B.; Solomon, E. I. *J. Biol. Inorg. Chem.* **2000**, *5*, 16.
(48) Sanders-Loehr, J. The CUA site of cytochrome c oxidase. In *Physical Methods in Bioinorganic Chemistry*; Que, L., Jr., Ed.; University Science Books: Sausalito, CA, 2000; p 505.
(49) Kroneck, P. M. H.; Binuclear Copper, A. In *Handbook of Metalloproteins*; Messerschmidt, A., Huber, R., Poulos, T., Wieghardt, K., Eds.; Wiley: Chichester, 2001; Vol. 2, p 1333.
(50) Lappalainen, P.; Aasa, R.; Malmström, B. G.; Saraste, M. *J. Biol. Chem.* **1993**, *268*, 26416.
(51) von Wachenfeldt, C.; de Vries, S.; van der Oost, J. *FEBS Lett.* **1994**, *340*, 109.
(52) Slutter, C. E.; Sanders, D.; Wittung, P.; Malmström, B. G.; Aasa, R.; Richards, J. H.; Gray, H. B.; Fee, J. A. *Biochemistry* **1996**, *35*, 3387.
(53) Williams, P. A.; Blackburn, N. J.; Sanders, D.; Bellamy, H.; Stura, E. A.; Fee, J. A.; McRee, D. E. *Nat. Struct. Biol.* **1999**, *6*, 509.
(54) Komorowski, L.; Anemuller, S.; Schafer, G. *J. Bioenerg. Biomembr.* **2001**, *33*, 27.
(55) Song, A.-X.; Li, L.-Z.; Yu, T.; Chen, S.-M.; Huang, Z.-X. *Protein Eng.* **2003**, *16*, 435.
(56) Paumann, M.; Lubura, B.; Regelsberger, G.; Feichtinger, M.; Koellensberger, G.; Jakopitsch, C.; Furtmueller, P. G.; Peschek, G. A.; Obinger, C. *J. Biol. Chem.* **2004**, *279*, 10293.
(57) van der Oost, J.; Lappalainen, P.; Musacchio, A.; Warne, A.; Lemieux, L.; Rumbley, J.; Gennis, R. B.; Aasa, R.; Pascher, T.; Malmström, B. G.; Saraste, M. *EMBO J.* **1992**, *11*, 3209.
(58) Dennison, C.; Vijgenboom, E.; de Vries, S.; van der Oost, J.; Canters, G. W. *FEBS Lett.* **1995**, *365*, 92.
(59) Hay, M.; Richards, J. H.; Lu, Y. *Proc. Natl. Acad. Sci. U.S.A.* **1996**, *93*, 461.
(60) Jones, L. H.; Liu, A.; Davidson, V. L. *J. Biol. Chem.* **2003**, *278*, 47269.
(61) Hay, M. T.; Ang, M. C.; Gamelin, D. R.; Solomon, E. I.; Antholine, W. E.; Ralle, M.; Blackburn, N. J.; Massey, P. D.; Wang, X.; Kwon, A. H.; Lu, Y. *Inorg. Chem.* **1998**, *37*, 191.
(62) Farver, O.; Lu, Y.; Ang, M. C.; Pecht, I. *Proc. Natl. Acad. Sci. U.S.A.* **1999**, *96*, 899.
(63) Robinson, H.; Ang, M. C.; Gao, Y.-G.; Hay, M. T.; Lu, Y.; Wang, A. H. J. *Biochemistry* **1999**, *38*, 5677.
(64) DeBeer George, S.; Metz, M.; Szilagyi, R. K.; Wang, H.; Cramer, S. P.; Lu, Y.; Tolman, W. B.; Hedman, B.; Hodgson, K. O.; Solomon, E. I. *J. Am. Chem. Soc.* **2001**, *123*, 5757.
(65) Epel, B.; Slutter, C. S.; Neese, F.; Kroneck, P. M. H.; Zumft, W. G.; Pecht, I.; Farver, O.; Lu, Y.; Goldfarb, D. *J. Am. Chem. Soc.* **2002**, *124*, 8152.

(66) Lukoyanov, D.; Berry, S. M.; Lu, Y.; Antholine, W. E.; Scholes, C. P. *Biophys. J.* **2002**, *82*, 2758.
(67) Xie, X.; Gorelsky, S. I.; Sarangi, R.; Garner, D. K.; Hwang, H. J.; Hodgson, K. O.; Hedman, B.; Lu, Y.; Solomon, E. I. *J. Am. Chem. Soc.* **2008**, *130*, 5194.
(68) Robinson, N. J.; Winge, D. R. *Annu. Rev. Biochem.* **2010**, *79*, 537.
(69) Sieracki, N. A.; Hwang, H. J.; Lee, M. K.; Garner, D. K.; Lu, Y. *Chem. Commun.* **2008**, 823.
(70) Wang, X.; Berry, S. M.; Xia, Y.; Lu, Y. *J. Am. Chem. Soc.* **1999**, *121*, 7449.
(71) Hwang, H. J.; Nagraj, N.; Lu, Y. *Inorg. Chem.* **2006**, *45*, 102.
(72) Nilges, M. J.; Matteson, K.; Belford, R. L. SIMPOW6: A software package for the simulation of ESR powder-type spectra. In *ESR Spectroscopy in Membrane Biophysics*; Hemminga, M. A., Berliner, L., Eds.; Springer: New York, 2006; Vol. 27, p 394.
(73) Wang, X.; Ang, M. C.; Lu, Y. *J. Am. Chem. Soc.* **1999**, *121*, 2947.
(74) Hwang, H. J.; Lu, Y. *Proc. Natl. Acad. Sci. U.S.A.* **2004**, *101*, 12842.
(75) Cavallini, D.; De Marco, C.; Dupre, S. *Arch. Biochem. Biophys.* **1968**, *124*, 18.
(76) Cavallini, D.; De Marco, C.; Dupre, S.; Rotilio, G. *Arch. Biochem. Biophys.* **1969**, *130*, 354.
(77) Pecci, L.; Montefoschi, G.; Musci, G.; Cavallini, D. *Amino Acids* **1997**, *13*, 355.
(78) Solomon, E. I.; Baldwin, M. J.; Lowery, M. D. *Chem. Rev.* **1992**, *92*, 521.
(79) Brown, K.; Djinovic-Carugo, K.; Haltia, T.; Cabrito, I.; Saraste, M.; Moura, J. J. G.; Moura, I.; Tegoni, M.; Cambillau, C. *J. Biol. Chem.* **2000**, *275*, 41133.
(80) St. Clair, C. S.; Ellis, W. R., Jr.; Gray, H. B. *Inorg. Chim. Acta* **1992**, *191*, 149.
(81) Van de Kamp, M.; Canters, G. W.; Andrew, C. R.; Sanders-Loehr, J.; Bender, C. J.; Peisach, J. *Eur. J. Biochem.* **1993**, *218*, 229.
(82) Maret, W.; Kozlowski, H. *Biochim. Biophys. Acta* **1987**, *912*, 329.
(83) Farrar, J. A.; Formicka, G.; Zeppezauer, M.; Thomson, A. J. *Biochem. J.* **1996**, *317*, 447.
(84) Maret, W.; Dietrich, H.; Ruf, H. H.; Zeppezauer, M. *J. Inorg. Biochem.* **1980**, *12*, 241.
(85) Maret, W.; Zeppezauer, M.; Desideri, A.; Morpurgo, L.; Rotilio, G. *FEBS Lett.* **1981**, *136*, 72.
(86) Siluvai, G. S.; Nakano, M. M.; Mayfield, M.; Nilges, M. J.; Blackburn, N. J. *Biochemistry* **2009**, *48*, 12133.
(87) Banci, L.; Bertini, I.; McGreevy, K. S.; Rosato, A. *Nat. Prod. Rep.* **2010**, *27*, 695.
(88) Belle, C.; Rammal, W.; Pierre, J.-L. *J. Inorg. Biochem.* **2005**, *99*, 1929.
(89) Solomon, E. I.; Xie, X.; Dey, A. *Chem. Soc. Rev.* **2008**, *37*, 623.
(90) Hu, J.; Dong, L.; Outten, C. E. *J. Biol. Chem.* **2008**, *283*, 29126.
(91) Abriata, L. A.; Banci, L.; Bertini, I.; Ciofi-Baffoni, S.; Gkazonis, P.; Spyroulias, G. A.; Vila, A. J.; Wang, S. *Nat. Chem. Biol.* **2008**, *4*, 599.
(92) Boal, A. K.; Rosenzweig, A. C. *Chem. Rev.* **2009**, *109*, 4760.